

Robust Power System Stabilizer Design

Devandren Moodley

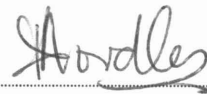
2002

University of Natal

Submitted in partial fulfillment (56%) of the academic requirements of the degree of Master of Science in the Department of Electrical Engineering, University of Natal, June 2002.

The work contained in this thesis is my own except where expressly stated as being referenced from other work. The work contained herein has not been submitted in part, or in whole to any other University.

The research work was conducted under the supervision of Professor E.S Boje and Dr. B.S Rigby.


.....

Dedicated to my parents, for their constant love and support

Acknowledgements

I would like to express my deepest gratitude to my supervisor, Professor E.S Boje, for the constant support and guidance afforded to me throughout the course of this thesis. Also deeply appreciated is the efforts made by Professor Boje during the correction of this document. I would also like to thank my co-supervisor Dr. B.S. Rigby for providing assistance with aspects in Power Systems. Discussions with Dr. P.S Rao, a visiting scholar of IIS-Bangalore (India), greatly enhanced understanding of the work undertaken.

I would also like to thank my family, without whom none of this would have been possible. To the post-graduate students of Electrical and Electronic engineering for provided the greatly needed diversions from the righteous path.

ABSTRACT

This thesis investigates the design of damping controllers to alleviate the problem of low frequency electro-mechanical oscillations in power systems. The operating point and network parameters of power systems are continually changing, resulting in changes in system dynamics. The conventional controller design methodology has therefore come under increasing scrutiny for its lack of considerations for robustness.

The thesis first outlines the conventional design of a power system stabilizer (PSS) and then applies two robust techniques (H_∞ and Quantitative Feedback Theory, QFT) to the design problem. The single machine infinite bus (SMIB) model is used to illustrate the procedure for all three design techniques. The final design is undertaken to illustrate the more important problem of robust multi-machine PSS design using QFT. The design requires linearised models of the multi-machine system. A brief discussion is given on how these can be obtained. An introduction to decentralized control design in QFT is included to support the multi-machine design.

Chapter three proceeds through the design steps required to generate a conventional PSS. The technique is shown to be simple for a given set of operating conditions. The controller is shown to be adequately robust over the given set of operating conditions albeit not by design.

Chapter four introduces a design technique that directly addresses robustness issues during the controller design. For a restricted range of operating conditions the designed controller demonstrates the desired robustness and performance characteristics. The inherent difficulties with H_∞ in PSS design become more apparent as the operating range is extended.

Chapter five introduces the second robust controller design technique. QFT is shown to be more adept at dealing with increased operating ranges and changing specifications in

the single-machine infinite-bus case. The controller is easy to generate and performs well over the entire range of operating conditions. QFT is also applied to the controller design for a four-machine study system. The design is a marginally more complex than in the single machine case but is still easily accomplished.

This thesis confirms previous attempts at solving the design problem using the methods outlined above. The performance of all controllers is assessed for small and large disturbances using non-linear time domain simulations with models developed using PSCAD/EMTDC and MATLAB.

CONTENTS

CHAPTER		PAGE
1.	Introduction	1
1.1.	General	1
1.2.	Background and objectives	2
1.3.	Thesis layout	3
1.4.	Software tools	4
1.5.	Achievements and findings	5
2.	Literature survey	7
2.1.	Introduction	7
2.2.	Review of the power system oscillatory mechanism	8
3.	Conventional design and tuning of PSS's	15
3.1.	Introduction	15
3.2.	Function of a PSS	16
3.3.	Design example	17
3.4.	Summary and conclusions	25
4.	On H_∞ PSS design	26
4.1.	Introduction	26
4.2.	Theory of H_∞	27
4.3.	Uncertainty modelling	30
4.4.	Selecting weighting functions	33
4.5.	The standard H_∞ problem	34
4.6.	H_∞ PSS design example	36
4.7.	Extending the range of operating conditions	42
4.8.	Summary and conclusions	44
5.	QFT applied to PSS design	45
5.1.	Introduction	45
5.2.	QFT tracking design for SISO systems	46
5.3.	Extending QFT to multi-variable systems	50

5.3.1. Diagonal controller design	50
5.4. QFT in SMIB PSS design	55
5.4.1. Design for a restricted range of operating conditions	55
5.4.2. Extending the range of operating conditions	61
5.5. Multi-machine PSS design	66
5.5.1. The four machine study network	66
5.5.2. The structured singular value as a stability measure	69
5.6. Design example	71
5.6.1. Stability boundary determination	72
5.6.2. Performance specification determination	74
5.7. Summary and conclusions	80
6. Conclusions	81
6.1. Comparative analysis	81
6.2. Suggestions for further work	82

APPENDICES

Appendix A – SMIB system modelling

Appendix B

Appendix B.1 – System data

Appendix B.2 – K constants

Appendix B.3 – System description for the extended range of operating Conditions

Appendix C – Glover-Doyle solution to the standard H_∞ problem

Appendix D

Appendix D.1 – Parameters of the two-area system

Appendix D.2 – The Power System Toolbox

LIST OF FIGURES AND TABLES

Figures

Fig 2.1: Block diagram of the third order linearised SMIB system

Fig 2.2: Rotor angle responses following a step change in mechanical torque

Fig 3.1: Block diagram of a simple PSS

Fig 3.2: Block diagram of transfer function from V_{ref} to ΔT_e

Fig 3.3: Linearised SMIB block diagram

Fig 3.4: Phase plots of $G_P(s)$ and $PSS(s)$

Fig 3.5: Bode magnitude plot of the open and closed loop plant

Fig 3.6: Closed loop system response to a 5% step disturbance at the AVR reference input for 100 ms

Fig 3.7: Closed loop system response to a three phase fault at the infinite bus for 100 ms

Fig 4.1: SISO system, output magnitude response

Fig 4.2: General perturbation model

Fig 4.3: Small gain condition represented on the Nyquist plane

Fig 4.4: Additive and multiplicative uncertainty model

Fig 4.5: Generalized plant model

Fig 4.6: SMIB block diagram with uncertainty blocks added

Fig 4.7: Magnitude plots of uncertainty transfer functions

Fig 4.8: Bode plot of the H_∞ PSS

Fig 4.9: Magnitude plot of the open loop plant $P(s)$ and the closed loop $L(s)$

Fig 4.10: Closed loop system response to a 5% step disturbance at the AVR reference input for 100 ms

Fig 4.11: Closed loop system response to a three phase fault at the infinite bus for 100 ms

Fig 4.12: Magnitude plots of uncertainty transfer functions for extended operating range

Fig 5.1: 2 DOF structure

Fig 5.2: Frequency domain boundary specifications with translation onto the Nichols chart

Fig 5.3: Boundary constraints plotted on the Nichols chart

Fig 5.4: Bode magnitude plot of output sensitivity vs design specifications

Fig 5.5: Boundary division for tracking design

Fig 5.6: Open loop plant characteristics

Fig 5.7(a): Boundary constraints for the SMIB system

Fig 5.7(b): Nominal plant with the controller added

Fig 5.8: Bode plot of the controller

Fig 5.9: Magnitude plot of the closed loop plant vs design specification

Fig 5.10: Closed loop system response to a 5% step disturbance at the AVR reference input for 100 ms

Fig 5.11: Closed loop system response to a three phase fault at the infinite bus for for 100 ms

Fig 5.12: Magnitude plots of the open loop transfer function matrix elements

Fig 5.13: Magnitude plots of the closed loop transfer function matrix elements with the PSS added

Fig 5.14: System responses to a 5% step disturbance at the AVR input for 100 ms

Fig 5.15: System responses to a three-phase fault at the infinite bus applied for 100 ms

Fig 5.16: Two-area test case

Fig 5.17: PSCAD/EMTDC implementation of the study system

Fig 5.18: Effect of the inter-area mode on tie-line power flow

Fig 5.19: Equivalent feedback structure

Fig 5.20: Magnitude of the elements of T , $-\frac{1}{\mu(M)}$

Fig 5.21: Nominal PSS with added perturbation

Fig 5.22: Stability bound on PSS response at the inter-area mode frequency

Fig 5.23: Magnitude plot of the plant element and plot of the modified function

Fig 5.24: Stability bounds and performance bounds

Fig 5.25: Designed controller plotted against the specifications

Fig 5.26: System responses to a 5% step disturbance at the AVR input of all
generators for 100 ms; case a-d

Fig 5.27: System responses to a three-phase fault at bus number 8 applied for 100 ms
case a-d

Tables

Table 4.1: Restricted range of operating conditions

Table 4.2: Extended range of operating conditions

Table 5.1: Operating conditions for the two-area test case

LIST OF SYMBOLS

External parameters

K_D	mechanical damping
P	generator terminal real power
Q	generator terminal reactive power
V_t	generator terminal voltage
V_b, E_b	infinite bus voltage
X_e	transmission line equivalent reactance

Synchronous generator parameters

E_t, V_t	generator terminal voltage
E_{fd}	generator field voltage
E_{q0}	pre-disturbance voltage behind $(R_a + jX_q)$
e_d, e_q	armature voltage
$E_{f \min}, E_{f \max}$	AVR voltage limits
$G_{exc}(s)$	exciter transfer function
$H = 0.5 * M$	inertia constant
i_d, i_q	armature current
i_{fd}	generator field current
i_{kd}, i_{kq}	damper winding currents
K_D	mechanical damping coefficient
K_{pss}	power system stabilizer gain
L_d, L_q	stator self-inductance
L_l	stator leakage inductance
L_{ad}, L_{aq}	mutual inductance
L_{fd}	field winding self-inductance
L_{kd}, L_{kq}	damper winding self-inductances
P_m	mechanical input power
R_a	armature resistance
R_{fd}	field winding resistance
R_{kd}, R_{kq}	damper winding resistance
T_e	electrical torque produced by the generator

T_{d0}', T_{q0}'	open circuit transient time constants
T_m	mechanical torque input
T_R	AVR feedback transducer time constant
T_w	washout block time constant
X_d, X_q	stator self inductive reactances
X_d'	d axis transient reactance
X_{ad}, X_{aq}	mutual reactances
X_{fd}	field winding self inductive reactance
X_{kd}, X_{kq}	damper winding self inductive reactances
X_l	stator leakage reactance
ψ_{fd}	field flux linkage
ψ_d, ψ_q	stator flux linkages
δ	rotor angular position
ω_r	rotor speed (rad/sec)
ω_0	nominal system frequency, 377 rad/sec (60 Hz)

The subscripts used throughout the text have the following meanings unless otherwise stated.

'd'	d-axis component
' θ '	denotes linearisation around a chosen nominal point
'q'	q-axis component
's'	saturated value of a quantity
'u'	unsaturated value of a quantity

The superscript ' \prime ' as applied to reactance's denotes the transient value of the quantity concerned.

ACRONYMS

AVR	Automatic voltage regulator
H_∞	H infinity
PSS	Power system stabiliser
QFT	Quantitative feedback theory
SMIB	Single machine infinite bus

CHAPTER ONE

INTRODUCTION

1.1 General

Inherent in large power system behaviour are phenomena termed local and inter-area modes. These are low frequency, poorly damped electro-mechanical oscillations, where generators in one area swing against each other (local mode), or generators of one area swing against generators of another area or the aggregate system (inter-area mode). Typical frequencies for these oscillations lie in the range of 0.2 to 3 Hz (Kundur, 1994; Rao, 1998a). Power transfer limits are severely restricted by these oscillations due the threat of network security compromise. The problem has been further aggravated by the use of fast acting automatic voltage regulators (AVR's) and long, weak transmission links.

Modulating the generator field excitation signal, in a coordinated manner using a supplementary control signal at the AVR input summing junction, has been identified as a means to effectively damp out these oscillations. The device used to achieve this is termed a power system stabiliser (PSS). The signals considered most feasible as inputs to such a device, are shaft speed, AC bus frequency, and a combination of terminal power and shaft speed (Larsen and Swann, 1981). The stabiliser output is fed back to the AVR input summing junction, with the appropriate gain and phase advance, to achieve the required degree of modulation of the field excitation signal. PSS's are traditionally designed as lead compensators and are largely contingency-based designs. The designs are undertaken for the operating condition possessing oscillations with the poorest damping. This restricts their effectiveness to a small region around the design operating point.

Traditional design techniques adopted by DeMello and Concordia (1969), Larsen and Swann (1981), Kundur (1994) and others have been successful in the past due to the limited range of operating conditions of power networks. With increased demand being placed on power networks, the feasible range of operating conditions has become larger. A consequence of this, is the operation of generators with reduced stability margins. These are changes required to meet the increasing demand for electricity without the need to build costly new generating units and transmission networks. Small signal stability has always been of paramount importance for any power network. This is the ability of a system to remain in synchronism following small disturbances (Swift, 1996a; Chonco, 2000).

The prospect of instability has necessitated the application of improved design techniques to endow PSS's with robustness properties so as to ensure sufficient damping over the entire range of operating conditions. Advances in robust control have introduced new techniques for the design of controllers possessing such robustness properties. All of these techniques are however not directly applicable to power systems.

H_∞ optimal control and Quantitative Feedback Theory (QFT) are two well researched and widely used methods for robust controller design. These will be discussed and applied to robust controller design in the course of this thesis.

1.2 Background and Objectives

For power systems constrained by stability concerns, the limiting factor is damping of system oscillations and not first swing stability (Swift, 1996a). The damping of these oscillations has traditionally been the task of a PSS and has received much attention in past work (DeMello and Concordia, 1969; Larsen and Swann, 1981; Kundur, 1994). These authors have presented a design technique for a PSS, which effectively adds

damping to these oscillations. The major drawback of controllers designed in this manner is the failure to adequately address robustness issues during the design process. The primary aim of this thesis is to highlight two robust design techniques for PSS design. The conventional design method is also presented for a SMIB system for completeness and to highlight the differences between the three design approaches. The robust design methodologies chosen are H_∞ optimal control and QFT. The latter is also applied to the design of a multi-machine stabiliser to address the issue of damping of inter-area mode oscillations in multi-machine networks. The work presented in this thesis follows from Rao (1998a) for H_∞ , Boje and Jennings (2001) and Rao and Boje (2001) for QFT. The performance of all stabilisers is assessed using the non-linear power system simulation package, PSCAD/EMTDC.

1.3 Thesis layout

This thesis consists of five further chapters and appendices. The material is arranged as follows.

A review of the literature on the application of PSS's to power system damping is presented in Chapter Two. The chapter begins by reviewing the conventional design and implementation of power system stabilizers and then extends this to the attempts at robust stabiliser design. The scope is focused to coincide with the methods used in later chapters of this thesis.

The conventional design technique for a SMIB PSS is outlined in Chapter Three. The design is accomplished by following and combining the work in references, Larsen and Swann, 1981; Kundur, 1994; Lakmeharan and Coker, 1999. The performance of the resulting PSS is assessed using a non-linear simulation (PSCAD/EMTDC).

Chapter Four makes the transition from conventional to robust design techniques. A brief outline of H_∞ theory is given to provide an introduction. The relevant extensions

and modifications for application to power systems are discussed. A stabiliser for a SMIB system operating over a restricted range of conditions is then synthesized with the H_∞ toolbox in MATLAB. An assessment of the controller performance is given using PSCAD/EMTDC. The work presented in this chapter closely follows Rao's (1998a) application of H_∞ to PSS design.

Chapter Five introduces QFT for both the general single input single output and multi-variable formulations of SMIB systems. Two PSS designs for a SMIB example are presented. A final design for a multi-machine PSS is then presented. A brief discussion of the study network is given to highlight the design problem. The structured singular value is introduced as an adequate measure for stability and is then used to calculate the stability boundaries in the multi-machine QFT PSS design. The controller performance assessments are also shown.

Chapter Six summarises the main results from the previous chapters and discusses the merits and de-merits of all the design techniques presented. Some suggestions for further work are also given.

1.4 Software tools employed in the thesis

The non-linear simulation of a SMIB system was implemented in PSCAD/EMTDC. This simulation was used for assessing the performance of the controllers designed for the restricted range of operating conditions for all three design methods. A non-linear simulation implemented using MATLAB provided by Rigby (2000), with the required alterations by the author, was used for the extended range of operating conditions of Chapter Five (Sect. 5.4.2).

PSCAD/EMTDC was also used to perform the non-linear simulations of the four-machine test system under different operating conditions for controller performance assessment.

The H_∞ toolbox in MATLAB was used to synthesize the controller for the design example of Chapter Four. Also used was MATLAB's QFT toolbox for the designs of Chapter Five.

The Power System Toolbox (Cherry Tree Scientific Software, 1993) is shown in Appendix D to be useful in generating linearised models of the four-machine test system.

A copy of all software developed and used in the course of this thesis is provided on the accompanying compact disc.

1.5 Achievements and findings of the thesis

This work has achieved the following:

- An in depth understanding of the electromechanical oscillatory phenomena in power systems gained from a review of the pertinent literature.
- An implementation of non-linear simulations in PSCAD/EMTDC and MATLAB to assess the performance of all the designed controllers.
- Demonstrated robust techniques applied to the successful design of power system damping controllers.
- The conventional design method was extensively researched to fully understand the design approach and a design was presented.
- Understanding in the fields of H_∞ and QFT applied to robust controller design.

- Demonstrated the performance of all designed controllers.
- Confirmed the results of previous attempts at applying all three design techniques to PSS design.
- Outlined a method to obtain linearised models of multi-machine power system networks (Appendix D).

CHAPTER TWO

Literature Survey and Review of Power System Oscillations

2.1 Introduction

Chapter One outlined one of the major problems facing large power networks and highlighted the use of a PSS as a possible solution. PSS's are supplementary control devices added to the generators in the system to provide increases in damping torque. This increase in damping torque has been shown (DeMello and Concordia, 1969; Larsen and Swann, 1981; Kundur, 1994), to enhance network stability by damping out the system oscillations.

All generators in a power network may not require the addition of a PSS to ensure adequate damping of the system oscillatory modes. The topic of optimal placement has been dealt with in numerous papers, to identify suitable locations for the addition of PSS's (Martins and Lima, 1990; Kundur, 1994; Lakmeharan and Coker, 1999). The identification of these optimal locations is often based on participation factors, which in essence are a measure of the degree to which a particular generator participates in a specified mode. It has been shown (Kundur, 1994) that generators with the highest participation in a specified mode may be fitted with PSS's to effectively damp out the mode without the requirement of damping contributions from other generators in the network. Optimal placement was not considered in the studies undertaken, primarily due to the small size of the multi-machine test system used in Chapter Five.

This chapter reviews the oscillatory phenomena experienced in power systems and introduces the design techniques for controllers to alleviate the problem. The extensions of the robust techniques required for application to power systems are also highlighted in the relevant chapters. Their application to power system stabiliser design is then presented.

2.2 Review and outline of solutions to the power system oscillatory mechanism

Power system electro-mechanical oscillations

Consider the third order linearised model of a single machine connected to an infinite bus via an external reactance (DeMello *et al*, 1969; Kundur, 1994), shown in Figure 2.1. The model illustrates manual excitation control. Damper winding effects are ignored in this discussion but may be accounted for if required. The physical meaning of all symbols used may be found in the list of symbols at the beginning of the thesis. A single line diagram of a single machine infinite bus (SMIB) system can be found in Appendix A (Fig A.1).

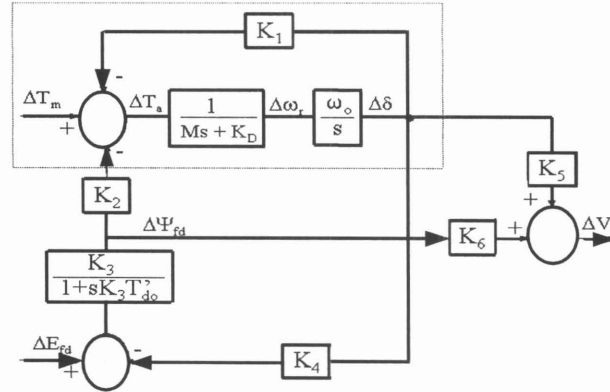


Figure 2.1: Block diagram of the third order linearised SMIB system

The section enclosed within the dashed box represents the condition with constant d-axis flux linkage and represents the mechanical dynamics and the external electrical network. To investigate the damping and synchronizing torques before the introduction of excitation control, a few simple concepts will be developed. The section enclosed by the dashed box in Figure 2.1 has a characteristic equation given by,

$$s^2 + \frac{K_D}{M}s + \frac{K_1\omega_0}{M} = 0 \quad 2.2.1$$

The natural frequency in equation 2.2.1 is, $\omega_n = \sqrt{(K_1 \omega_0) / M}$ and the damping ratio is, $\zeta = 0.5 K_D / \sqrt{K_1 M \omega_0}$. At any oscillatory frequency the accelerating torque (ΔT_a) in Figure 2.1 is comprised of two components, one in phase with the machine rotor angle (synchronizing torque) and the other in phase with the machine rotor speed (damping torque), (DeMello *et al*, 1969; Kundur, 1994). The accelerating torque oscillations can always be broken down into these two components. A positive synchronizing torque is always desirable as this ensures that the rotor angle is restored to the equilibrium position following a small perturbation. Including the de-magnetising effect of the armature reaction, which is the forward path through the element K_4 , the electrical torque contribution is,

$$\Delta T_e = \frac{-K_2 K_3 K_4}{1 + s K_3 T'_{do}} \Delta \delta \quad 2.2.2$$

As the constants K_i , $i = 2 \dots 4$, are always positive, it is clear that the demagnetising effect has a negative contribution to the synchronizing torque component at steady state ($s = 0$). At an oscillatory frequency of $\omega \gg 1/(K_3 T'_{do})$, the phase of the torque described by equation 2.2.2 changes to +90 degrees, and it is in phase with the rotor speed. It therefore has a purely damping effect. DeMello *et al* (1969) show that for typical oscillation frequencies of about one hertz the field contribution to the damping ratio would be between 0.03 - 0.05 %.

Figure 2.2 illustrates the response of the rotor angle, for the system of Figure 2.1, following a small step disturbance in the mechanical torque with K_D equal to zero. In Figures 2.2(a) and 2.2(b) the field flux variation is zero. The response for K_1 positive and negative is shown in Figure 2.2(a) and 2.2(b) respectively. Figures 2.2(c) and 2.2(d) show the response with the change in field voltage equal to zero, and the total synchronizing torque coefficient, $K_s = K_1 - K_2 K_3 K_4$, positive and negative respectively. The effect on the damping and synchronizing torque components when a

high gain automatic voltage regulator (AVR) is added to the system is shown in Chapter Three (eq. 3.2.2).

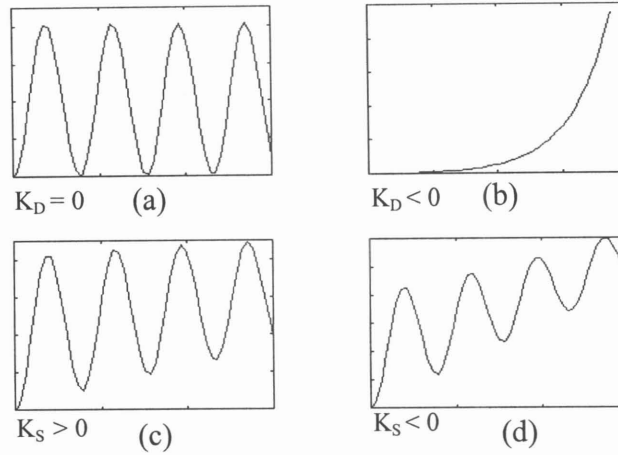


Figure 2.2: Rotor angle responses following a step change in mechanical torque

DeMello *et al* (1969) explains the need for restricting the AVR transient gain due to open-circuit considerations when the machine angle has no significance. It is at times desirable to have high gain for steady-state operation while restricting the transient gain as discussed above. If a high gain regulator is used to satisfy the gain requirements for steady-state operation, a reduction in the transient gain can be achieved by adding a lag network in series with the regulator, or with rate feedback from the exciter voltage. A high gain exciter also serves to almost eliminate the negative steady-state synchronizing torque coefficient produced by the de-magnetising effect of armature reaction. The damping component of this torque is correspondingly reduced. A high gain voltage regulator provides improvement in the synchronizing torque but this is to the detriment of the natural damping of the machine. This results in oscillatory behaviour of the machine for some operating conditions. An effective way to solve the problem of poorly damped modes is to provide a stabilising signal derived from machine speed, terminal frequency, power or combinations of signals.

Power system stabilisers

Larsen and Swann (1981) discuss the application and tuning of the devices (PSS) described above. The PSS is required to produce a component of electrical torque in phase with the rotor speed deviations. Regardless of the input signal chosen, the stabiliser is required to compensate for the gain and phase characteristics of the excitation system, the generator and the power system. Practical speed input stabilisers must have high frequency, gain attenuation to limit the impact of noise and minimise torsional inter-action (Larsen and Swann, 1981). This can be accomplished by utilising low-pass or band-reject filters. Also introduced is a washout stage to prevent steady-state terminal voltage changes as the system frequency changes. The design of a PSS utilising rotor speed deviations as input, is given in Chapter Three. The root locus is shown by Larsen and Swann (1981) to be a convenient and effective way to tune the stabiliser gain for optimum damping.

Lakmeeharan and Coker (1999), have outlined a procedure for the optimal placement and tuning of PSS's. The tuning approach used is similar to the discussions given above. The formulae to enable the physical parameter calculations for the PSS lead and lag time constants are also given. A case study of inter-area mode damping is also presented.

In a paper by Klein, Rogers and Kundur (1991), the phenomenon of local and inter-area mode oscillations was considered. The concept was developed for a simple four generator, two-area test system. An investigation was performed to determine the effect of excitation systems used on system damping. If a fast exciter was used on one unit, with slow exciters on the other units, it was found that with a fast exciter in the receiving area the damping of the mode is significantly improved. A fast exciter in the sending area has the opposite effect. The location of the fast exciter also has an effect on the frequency of the mode. The effect of different generator and excitation models on the mode shape was investigated. For symmetric systems with no power flow across the tie line it was found that the generating units in one area oscillate in anti-phase with

those in the second area, regardless of generator and exciter characteristics. Generator and exciter characteristics are shown to be of a greater consequence for systems under high loading. Non-linear, static or dynamic loads are shown to have more of an impact on the inter-area mode in a stressed system and in a system with slow exciters. In a follow-up paper (Klein, Rogers, Moorthy and Kundur, 1992), an analytical investigation of the factors influencing PSS performance was performed. The effect of system loads, PSS location and the voltage characteristics are shown to be the key factors in determining PSS performance.

A major concern with respect to the controller design method used in the discussion above is the lack of robustness considerations during the design. A robust controller has the ability to perform satisfactorily over a broad range of operating conditions. The conventionally designed controller may display robustness once designed, but this is not incorporated into a systematic design procedure. There have been various attempts at applying robust techniques to damping controller design in power systems, and two of these techniques are discussed below.

H_∞ optimal control in power system stabiliser design

Klein, Xe, Rogers, Farrokhpay and Balu (1994) used H_∞ to design robust damping controllers for a large power system. The objective was to damp out the inter-area mode oscillation. It is shown in this paper that success of the designed controller relies on a reduced order system model and good engineering insight when the design specifications are chosen. The choice of the weighting functions plays a key role in determining the effectiveness of the resulting controller. The deviations in frequency response of the closed loop transfer function over the range of operating conditions can be represented as an uncertainty disk around a chosen nominal plant case.

Ahmed, Chen and Petroianu (1996) develop a method for decentralized H_∞ controller design. The method of balanced truncation is used to reduce the order of the synthesized controllers. An optimal controller is synthesized in the same manner as

given in the reference Klein *et al* (1994). The controller is found to achieve the design objectives with respect to H_∞ norm specifications but is ineffective in improving the damping factor of the closed loop poles, which is what was desired. A sub-optimal approach is presented to overcome this problem. This approach relies on creating a fictitious unstable plant by shifting the imaginary axis in the complex plane. The standard H_∞ algorithm is then applied to the new fictitious plant to generate a sub-optimal controller. The controller generated in this manner is shown to have superior performance to the controller synthesized using the conventional H_∞ formulation. This new technique is shown to produce controllers displaying the desired improvements in damping.

Cui, Ukai, Kando, Nakamura and Fujita (1999) present a decentralized controller design for a large system using H_∞ . The approach is similar to Klein *et al* (1994). Rao (1998a) develops the simplest formulation of applying H_∞ to the design of a damping controller for a single machine infinite bus system. The standard theory is extended to deal with representing plant uncertainty in a meaningful way as applied to power systems. The concept of H_∞ optimal controller design is further investigated in Chapter Four with a discussion of the modifications required for power system application.

Quantitative Feedback Theory (QFT)

Another approach to robust controller design is Quantitative Feedback Theory (QFT) introduced by Horowitz (1979, 1993). The ease of application of QFT to controller design makes it highly attractive. Some adaptation may be required for multi-machine PSS design. Rao (1998a,b) applies this philosophy to a PSS design for a single machine infinite bus (SMIB) system. An extension, based on the ideas of commutative controllers is made to enable the design of multi-machine stabilisers. This method places a restriction on the structure of the controller. A further modification is presented to circumvent the above restriction. The approach relies on robust non-singularity checks for complex interval matrices, coupled with solution of an optimisation problem for the controller parameters. A PSS and a supplementary damping controller for a mid-

point static var compensator (SVC) in a SMIB system, is designed to illustrate the ideas developed. Sedigh and Alizadeh (1994), propose the use of state-feedback to stabilise an unstable plant. A controller is then designed using QFT to satisfy the performance requirements. The essence of QFT is not fully exploited in that both problems can be approached simultaneously.

Boje and Jennings (2001), approach the problem of PSS design in a SMIB case from a multi-variable standpoint. The effects on the speed and voltage loops are determined after a PSS is added in the feedback path. The PSS is shown to affect only a cross-coupling term in the model description. This makes sense since the term mentioned is the transfer function relating the speed output to the AVR input, which is what is desired. Boje, Nwokah and Jennings (1999), shows a SMIB PSS can be designed to reduce the inter-action between the mechanical and electrical loops before feedback loop design of the AVR and governor loops are attempted. The Perron root is used a measure of inter-action between the diagonal and off-diagonal elements of the describing matrix. A return path decoupler is designed to reduce the inter-action index. This is a 'pre-controller' that has elements only on the off-diagonal, in the position where an effect is desired on the plant matrix.

The structured singular value in QFT design

Yang, Zhang and Yu (1999) introduced a new method for decentralized PSS design based on application of the structured singular value (SSV). The SSV was used to make conclusive deductions on system stability. Rao and Boje (2001) incorporated the use of the SSV stability measure into a multi-machine decentralized stabiliser design using QFT. A simple approach is developed to design the stabilisers for a single machine at a time. The ideas introduced by Yang, *et al* (1999), and used by Rao and Boje (2001), are further investigated and applied to multi-machine controller design in Chapter Five.

CHAPTER THREE

Conventional design and tuning of Power System Stabilisers (PSS)

3.1 Introduction

Numerous accounts of power system stabiliser design have been given throughout the last four decades (DeMello & Concordia, 1969; Larsen & Swann, 1981). This chapter serves to illustrate a conventional method for power system stabiliser design and tuning and its effect on the damping of low frequency poorly damped oscillations.

The major shortcoming of such design methods is their lack of quantifiable robustness during the design process over the entire feasible range of operating conditions for power systems. The subsequent chapters of this thesis outline design methodologies for controllers that possess such robustness properties. Performance analysis of all the designed controllers is provided in the relevant chapters.

The primary objective of this chapter is to provide a design and tuning technique for conventional PSS's and to illustrate their performance. The design method presented here follows from Kundur (1994) and is integrated with work undertaken by Lakmeeharan and Coker (1999). Chapter Two presented a review of some of the most influential papers on conventional controller design.

3.2 Function of a PSS

The primary function of a PSS is to add a component of damping torque in phase with rotor speed deviations, at the rotor oscillatory frequency. This is achieved by modulating the exciter input signal, with a supplementary signal applied at the automatic voltage regulator (AVR) input summing junction. This signal is obtained from the output of a supplementary control device, a PSS in this discussion. As mentioned earlier in this thesis, there exist numerous possibilities for input signals to such a device. In this and subsequent chapters, the rotor speed deviation is considered as the input. The block diagram of a simple PSS is shown in figure 3.1.

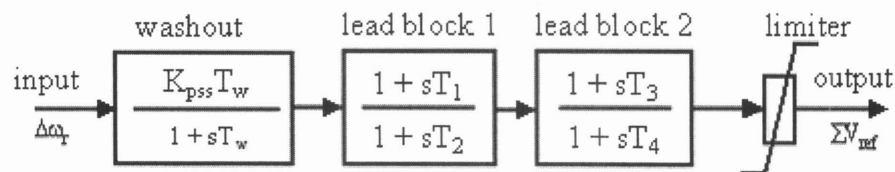


Figure 3.1: Block diagram of a simple PSS

The washout block is included to prevent steady changes in speed from modifying the terminal voltage. The K_{pss} term in figure 3.1 is used to tune the PSS gain to provide maximum damping. The phase compensation blocks are required to provide phase lead to compensate for the phase lag of the generator transfer function between the exciter input summing junction and electrical torque (ΔT_e), as shown in figure 3.2.

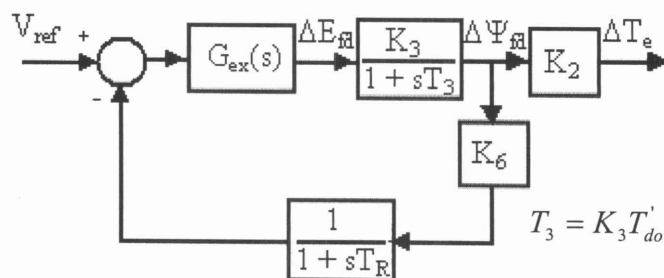


Figure 3.2: Block diagram of transfer function
from V_{ref} to ΔT_e

Figure 3.2 represents the AVR loop together with the excitation system of the linearised SMIB block diagram (Appendix A.1). Each phase lead block of the PSS in Figure 3.5 can provide a maximum of sixty degrees phase lead. Multiple blocks are used if the required phase lead is greater than sixty degrees.

3.3 Design example

The initial step is to investigate the effect of the AVR on the damping and synchronizing torque components of the generator. The change in electrical torque due to changes in field-flux linkage is given by equation 3.3.2. At steady state ($s = 0$), the torque component is in phase with the rotor position deviation. At any electromechanical oscillatory frequency ($s = j\omega$), the torque changes to be almost entirely in phase with the rotor speed deviations. From the block diagram of figure 3.3, it can be seen that the field flux variations due to changes in rotor position (Kundur, 1994; p 762) is given by,

$$\Delta\psi_{fd} = \frac{-K_3[K_4(1+sT_R)+K_5G_{ex}(s)]}{s^2(T_3T_R)+s(T_3+T_R)+(1+K_3K_6G_{ex}(s))}\Delta\delta \quad 3.3.1$$

The contribution to the electrical torque component due to changes in field flux linkage is thus given by,

$$\Delta T_e|_{\Delta\psi_{fd}} = \frac{-K_2K_3[K_4(1+sT_R)+K_5K_a]}{s^2(T_RT_3)+s(T_R+T_3)+(1+K_3K_aK_6)}\Delta\delta \quad 3.3.2$$

The function $G_{ex}(s)$ in equation 3.3.1 represents the transfer function of the excitation system. In equation 3.3.2 this has been replaced by K_a , which is the transfer function of a high gain excitation system (Kundur, 1994). The constants K_2 , K_3 , K_4 and K_6 are usually positive; K_5 can be either positive or negative (Kundur, 1994). These constants are dependent on the system and machine impedances and the operating condition

(DeMello and Concordia, 1969). It has been shown that the effect of the AVR on damping and synchronising torque components are most influenced by K_5 and $G_{ex}(s)$, (Kundur, 1994). If K_5 is positive, the AVR adds negative synchronising torque and positive damping torque and vice versa for K_5 negative. The design is now illustrated for Case One given in Table 3.1. The generator data is given in Appendix B.1 with the calculated K constants for the chosen example in Appendix B.2.

Case	P_b	Q_b	X_e
1	1.0	0.2	0.2
2	1.0	-0.2	0.3
3	1.0	0.5	0.3

Table 3.1: SMIB operating conditions

At the electromechanical mode frequency of $s = j\omega$ ($= j9.5345$ for case one, with the numerical values for $K_i, i = 1,2 \dots 6$, from Appendix B.2), equation 3.3.2 becomes,

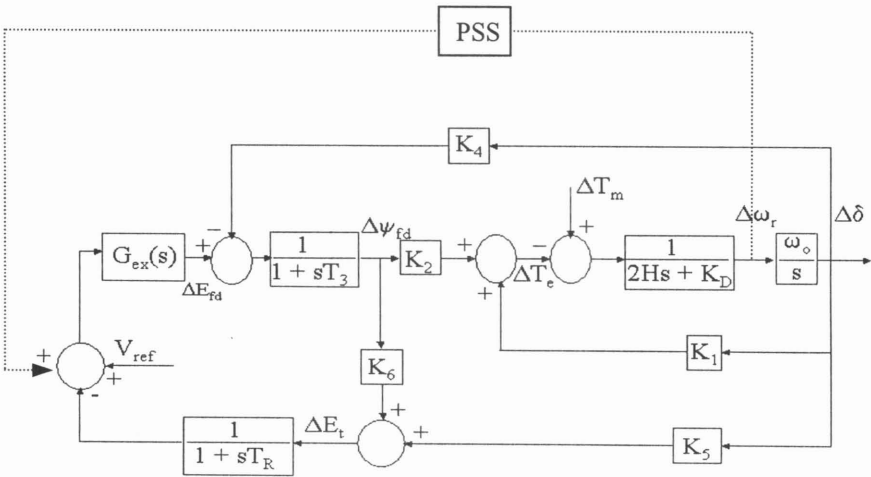


Figure 3.3: Linearised SMIB block diagram with PSS.
..... PSS signal path

$$\Delta T_e = \frac{-0.005812 \times j9.5345 + 0.0939}{0.01889 \times (j9.5345)^2 + 1.899 \times (j7.7836) + 12.63} \Delta \delta$$

$$= 0.0045 \Delta \delta - 0.0025(j\Delta \delta)$$

The synchronising torque component due to field flux variations is thus given by,

$$K_s = 0.0045 \text{ p.u. torque/rad}$$

and the damping torque component is given by,

$$K_D = \frac{-0.0025 \times \omega_o}{\omega} \Delta \omega_r$$

$$= -0.0989 \text{ p.u. torque/speed change}$$
3.3.3

To determine the phase lead that the PSS is required to provide, the phase lag from the exciter input to the electrical torque must first be determined. Including the effect of the voltage transducer time constant T_R , the transfer function from the exciter input to the electrical torque is given by equation 3.3.4,

$$\frac{\Delta T_e}{\Delta v_{PSS}} = G_P = \frac{K_2 K_3 K_a (sT_R + 1)}{s^2 (T_3 T_R) + s(T_3 + T_R) + (1 + K_3 K_6 K_a)}$$
3.3.4

Usually the time constant T_R is small with respect to other time constants in the circuit and its effect may be ignored resulting in,

$$\frac{\Delta T_e}{\Delta v_{PSS}} \approx G_P = \frac{K_2 K_3 K_a}{sT_3 + (1 + K_3 K_6 K_a)}$$
3.3.5

Equation 3.3.5 may now be used to calculate the phase lag from exciter input to electrical torque. Equation 3.3.5 produces a result that is approximately one degree less than equation 3.3.4 in this example, illustrating that neglecting the effect of T_R does not introduce gross error. At the rotor oscillation frequency given above, equation 3.3.5 gives,

$$G_P = \frac{45.11}{12.63 + j19.7745}$$

$$= 1.9 \angle -57.4^\circ$$

A rule of thumb is to compensate the phase lag to about ten degrees less than the actual amount required, thereby allowing for uncertainties in modelling and to ensure that the PSS does not negatively affect synchronising torque (Lakmeharan and Coker, 1999). The required phase lead for the design example is therefore chosen to be 47.5 degrees. The amount of damping introduced depends on the gain of the PSS transfer function at the rotor oscillation frequency. This gives the following result for the improvement in damping torque,

$$\Delta T_{PSS} = (\text{gain of PSS at } \omega = 9.5345) \times (1.922) \Delta \omega_r$$

From the value for K_D in equation 3.3.3, the minimum gain of the PSS required to combat the effect of armature reaction must be,

$$\text{gain}_{PSS_MIN} = \frac{0.0989}{1.922} = 0.052$$

Two lead blocks are used with each providing 23.75 degrees. One lead block would have sufficed for this design example since the required phase lead is less than 60 degrees. The PSS parameter calculations now proceed as follows (Lakmeharan & Coker, 1999). If the required phase lead for block 'i' is θ_m we have,

$$\sin(\theta_m) = \frac{a_i - 1}{a_i + 1} \quad 3.3.6$$

For the i 'th block, with the T_{2i-1} element associated with the zero of the lead block, this gives,

$$a_i = \frac{T_{2i-1}}{T_{2i}} \quad 3.3.7$$

and

$$\omega_m = \frac{1}{(\sqrt{a_i})T_{2i}} \quad 3.3.8$$

where ω_m is the frequency of the oscillatory mode.

Using the above information the following values for the time constants are obtained,

$$T_1 = T_3 = 0.1643 \text{ s}$$

$$T_2 = T_4 = 0.0667 \text{ s}$$

Figure 3.4 shows the $Arg(G_P(j\omega))$ of the generator, compared to the $Arg(PSS(j\omega))$. The washout term has not been included in the PSS description at this point. To prevent steady-state changes in terminal voltage as the system frequency changes, a washout filter is added as part of the final PSS transfer function. This is typically chosen as a high pass filter with the time constant being between one and twenty seconds (Kundur, 1994). The choice of the washout term is not critical with respect to PSS performance, but has an effect on the voltage loop. The time constant in this example is chosen to be five seconds. The gain of the PSS with $K_{PSS} = 1$ p.u., at the rotor frequency is 2.57. This illustrates that the PSS provides sufficient gain to combat the effect of the AVR.

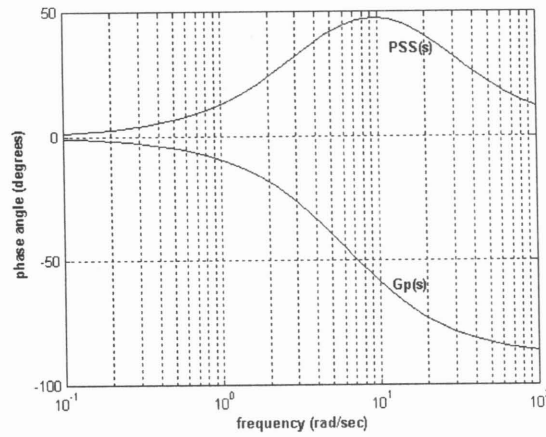


Figure 3.4: Phase plots of $G_p(s)$ and $PSS(s)$

The final PSS including the washout term thus has the following form,

$$PSS = \frac{5s}{(1+5s)} \frac{(1+0.165s)}{(1+0.0668s)} \frac{(1+0.165s)}{(1+0.0668s)}$$

The gain term K_{pss} does not have an infinite range over which the PSS remains stabilising. There exist values of K_{pss} where the PSS will destabilise the system. The PSS provides maximum damping at an optimum gain, K_{opt} . The gain, K_{pss} , may be tuned to find K_{opt} and achieve optimum damping, using the root locus (Larsen and Swann, 1981). The gain was not tuned for optimum damping in this example. Bode magnitude plots of the open and closed loop system, for all plant cases, are shown in figure 3.5. Non-linear simulations using PSCAD/EMTDC were performed to assess the controller performance. The small signal performance of the PSS is shown in figure 3.6 with the large disturbance response shown in figure 3.7. It is clearly visible that the controller is robust over the range of chosen operating conditions. Although this is desirable, the issue of robustness was not accounted for in the design process. In the example presented, the chosen operating conditions produce large differences in the magnitude peaks of the open loop system at their respective oscillatory frequencies, which may account for the eventual PSS being robust.

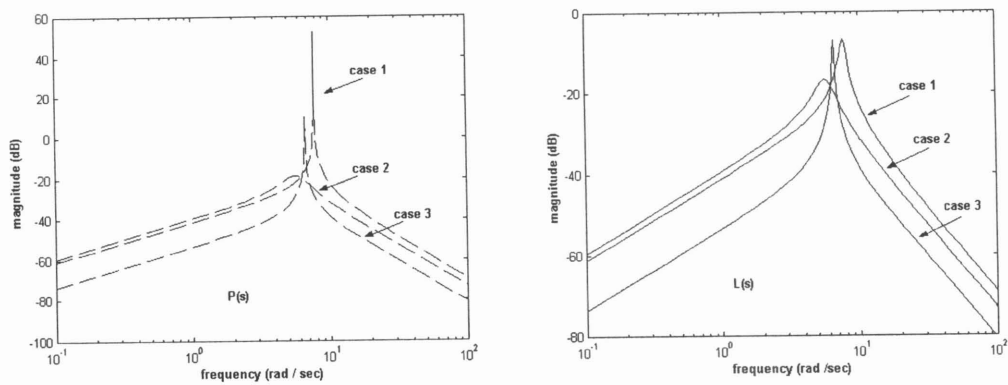


Figure 3.5: ‘----’ Bode magnitude plot of the open loop plant ($T_{\Delta\omega_r/V_{ref}}$);
— Bode magnitude plot of the closed loop plant ($T_{\Delta\omega_r/V_{ref}}$)

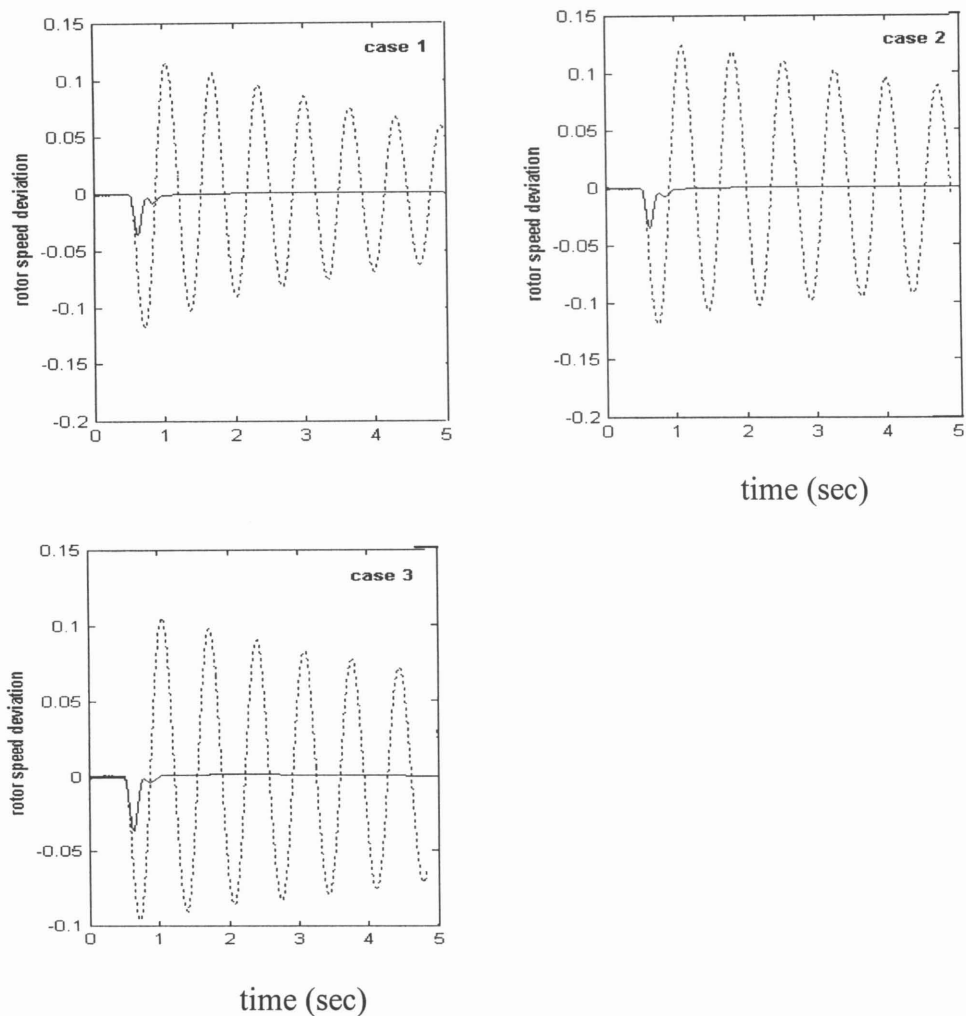


Figure 3.6: Closed loop system response to a 5% step disturbance at the AVR reference input for 100 ms ($T_{\Delta\omega_r/V_{ref}}$)
..... no PSS
— with PSS

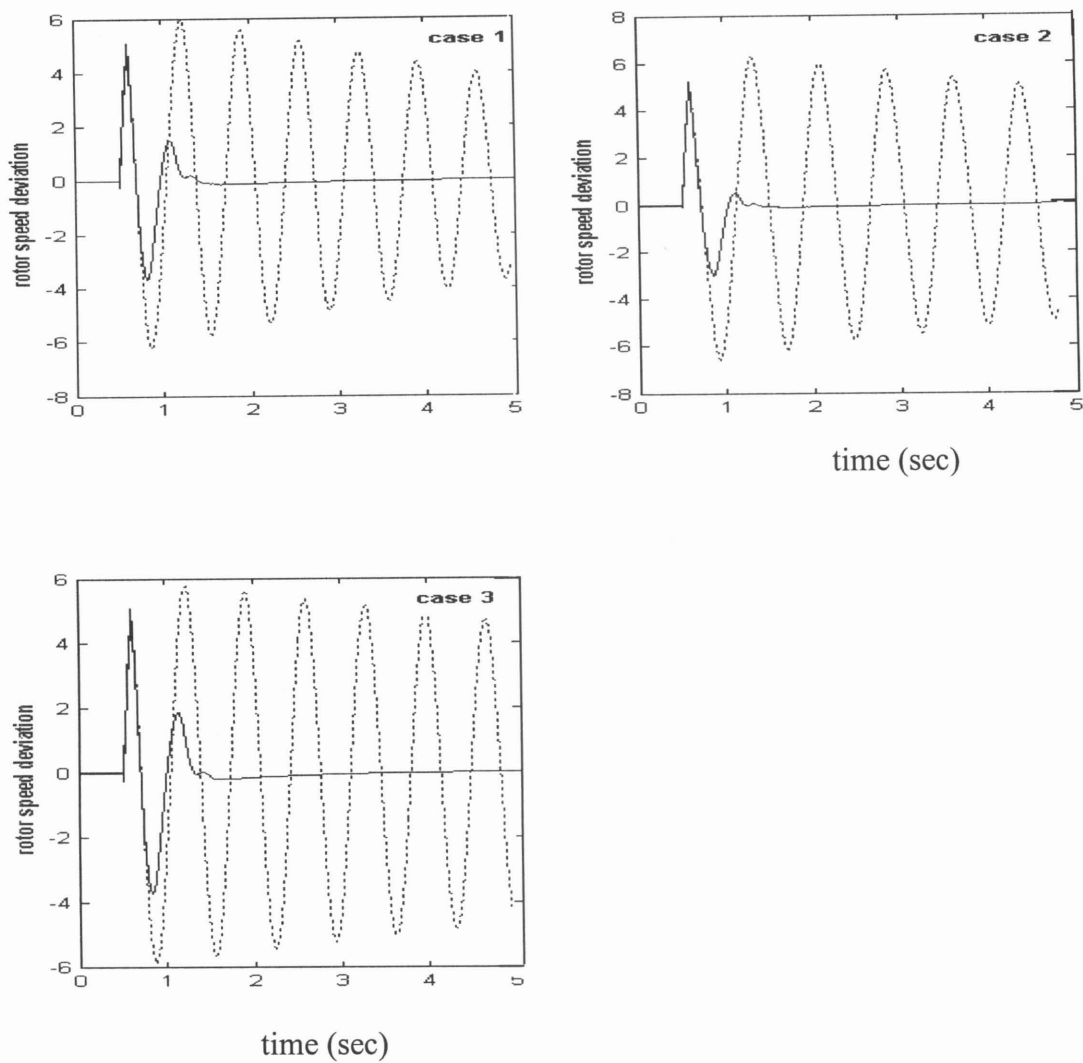


Figure 3.7: Closed loop system response to a three phase fault at the infinite bus cleared after 100 ms ($T_{\Delta\omega_r} / V_{ref}$)

.... no PSS

— with PSS

Saturation of the AVR signal produces responses similar to those illustrated in Figure 3.7. This was however not the case in these studies. Any improvement in damping was a direct consequence of the introduction of the PSS. In a complete research study the large signal behaviour may be investigated more thoroughly for a range of operating conditions.

3.4 Summary and conclusions

This chapter outlined the design of a conventional PSS applied to a SMIB system. The design approach is simple, requiring only that a worst case operating condition can be identified. The PSS is then designed to provide optimum damping for the worst case, with the view that all other plant cases will be sufficiently well damped. In the example presented it is seen that the controller has the desired performance for all operating conditions.

The approach presented in this chapter works well for the SMIB case. It has however been shown that improperly tuned controllers of this type, when applied to multi-machine systems can de-stabilise the lower frequency inter-area mode (Djukanovic, Khammash and Vittal, 1998).

The following chapters explore robust techniques for damping controller design. Within the H_∞ framework the problem is formulated as a nominal plant with an appropriate description of the uncertainty. This accounts for the parameter variation of the plant model with changing operating conditions. QFT addresses the problem of plant model variations with operating condition by requiring the formation of a template that contains all possible plant models. The controller is then designed to satisfy specifications at each frequency and for all plant models simultaneously.

CHAPTER FOUR

H_∞ based PSS design

4.1 Introduction

The concept of H_∞ optimal control for robust controller design was first introduced by Zames in the 1960's (Kwakernaak, 1993). The approach allowed for design with robustness considerations, far more directly than other optimisation methods. It made possible the synthesis of feedback systems, with guaranteed robust stability, in the presence of norm bounded uncertainty. The most widely accepted solution to the standard H_∞ problem is the state space solution developed by Glover and Doyle (Maciejowski, 1989).

There have been numerous attempts at designing controllers for power system application within the H_∞ framework (Klein, Le, Rogers, Farrokhpay and Balu, 1994; Ahmed, Chen and Petroianu, 1996; Rao, 1998a and Cui, Ukai, Kando, Nakamura and Fujita, 1999). Rao, (1998a) outlines some important considerations when applying H_∞ to general controller designs. The key issues are the choice of weighting function and avoiding pole-zero cancellations in the mixed sensitivity formulation. It has been observed that all the plant stable poles are cancelled by the controller zeros in the optimal solution to the mixed sensitivity formulation. The choice of weighting function requires good engineering insight into the design problem to ensure suitable controller synthesis for realistic design specifications.

This chapter outlines the design of a power system stabiliser (PSS) employing H_∞ concepts, for a single machine infinite bus (SMIB) system. The design is undertaken for the operating range given in Chapter Three. The performance of the PSS is assessed with a non-linear time domain simulation, implemented in PSCAD/EMTDC. The range of operating conditions has been restricted but can be extended with the relevant modifications to the problem definition.

4.2 Theory of H_∞

A brief outline of H_∞ theory is now provided. For a detailed discussion the reader should consult the relevant literature (Maciejowski, 1988; Kwakernaak, 1993; Limebeer and Green, 1993).

Consider the single input single output (SISO) system in fig 4.1, with the plant P containing no uncertainty. The closed loop transfer function is given by $T(s)$.

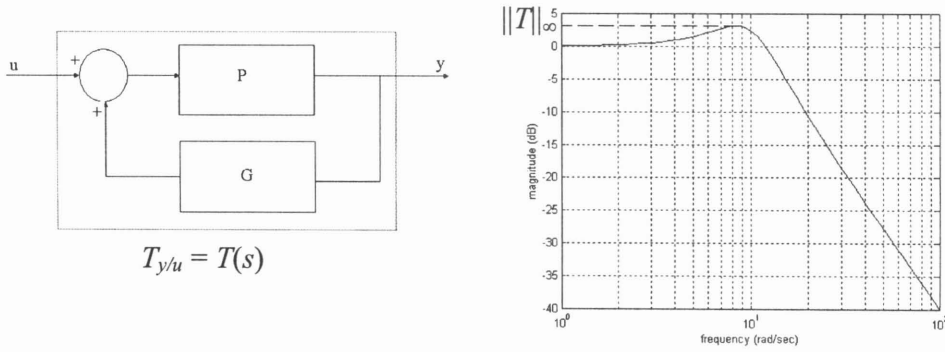


Figure 4.1: SISO system, output magnitude response

The infinity norm of a stable $T(j\omega)$ is defined as,

$$\|T(j\omega)\|_\infty = \max_{\omega} |T(j\omega)| \quad 4.2.1$$

which is the maximum magnitude of $T(j\omega)$ over all ω . If $T(j\omega)$ does not have a maximum value but is asymptotically close to some maximum value, equation 4.2.1 can be rewritten as follows,

$$\|T(j\omega)\|_\infty = \sup_{\omega} |T(j\omega)| \quad 4.2.2$$

This is the supremum or least upper bound of $T(j\omega) \forall \omega$. As a consequence of H_∞ belonging to the Hardy space of functions, $T(j\omega)$ is stable if $\|T(j\omega)\|_\infty$ has a finite maximum value. The Hardy space is a set of functions on the complex plane that are

both analytic and bounded in the right-half plane (Kwakernaak, 1993). If $\|T(j\omega)\|_\infty$ is infinite, $T(j\omega)$ is unstable by the same argument.

Equations 4.2.1 and 4.2.2 can be extended to deal with the multivariable case as follows. Here $\mathbf{G}(s)$ will be a matrix of transfer functions. Each element is a rational transfer function element. We thus have the following,

$$\|\underline{\mathbf{G}}(s)\|_\infty = \max_{\omega} \bar{\sigma}(\underline{\mathbf{G}}(j\omega)) \quad 4.2.3$$

This is the frequency dependent *maximum principal gain* of $\mathbf{G}(j\omega)$, in any direction. Hence, the *maximum principal gain*, $\bar{\sigma}(\bullet)$, gives the peak value over all frequencies of the worst-case gain of the matrix $\mathbf{G}(s)$.

Returning to the SISO case. If the maximum magnitude of $T(j\omega)$ is required to be limited by a weighting $W(\omega)$, where $W(\omega)$ is used to place an upper bound on the magnitude of $T(j\omega)$, over all frequencies such that,

$$|T(j\omega)| < W(\omega) \quad \forall \quad \omega \quad 4.2.4$$

or

$$|T(j\omega)| \times W^{-1}(\omega) < 1 \quad 4.2.5$$

From the sub-multiplicative property of matrix norms, ($\|\underline{\mathbf{A}} \times \underline{\mathbf{B}}\|_\infty \leq \|\underline{\mathbf{A}}\|_\infty \times \|\underline{\mathbf{B}}\|_\infty$), the following statement can be made,

$$\max_{\omega} |\underline{\mathbf{T}}(j\omega) \times \underline{\mathbf{W}}^{-1}(\omega)| \leq \max_{\omega} |\underline{\mathbf{T}}(j\omega)| \times \max_{\omega} |\underline{\mathbf{W}}^{-1}(\omega)| \quad 4.2.6$$

Combining equations 4.2.5 and 4.2.6 a matrix equivalent to the infinity norm specification can be written as follows,

$$\| T(j\omega) \times W^{-1}(\omega) \|_\infty < 1 \quad 4.2.7$$

The H_∞ norm bounded approach can thus be used to specify upper bounds on system functions. Possible applications include disturbance attenuation and closed loop performance specifications.

This brief discussion only serves to introduce H_∞ as used in a robust stability approach. An approach is now presented which makes use of the above arguments to illustrate the use of the infinity norm when applied to plants subject to uncertainty.

The SISO general plant perturbation model is shown in figure 4.2 with the plant P and the uncertainty Δ . The signals ' q ' and ' p ' are the inputs and outputs to the uncertainty respectively.

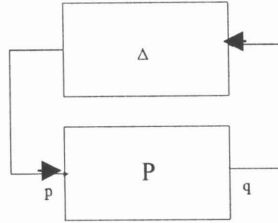


Figure 4.2: General perturbation model

If $P(s)$ is stable and $\Delta(s)$ is stable, the small gain theorem guarantees stability of the closed loop if the magnitude of the loop transmission, $L=P\Delta$, is less than unity. This is formulated using the infinity norm as follows,

$$\| P \times \Delta \|_\infty < 1 \quad 4.2.8$$

An interpretation of the above statement on the Nyquist plane is: The Nyquist plot of the maximum characteristic gain locus of the loop transmission cannot encircle the $(-1+j0)$ point thereby ensuring stability. Thus the contour is confined to the circle shown in figure 4.3.

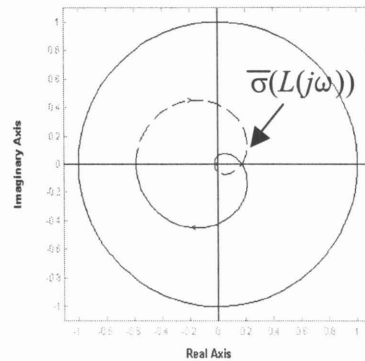


Figure 4.3: Small gain condition represented on the Nyquist plane

This leads to gross conservatism for plants whose Nyquist contour lies outside the circle but never encircles the $(-1+j0)$ point. Equation 4.2.8 can however, be used as a test for robust stability, by re-arranging a given plant structure to be equivalent to that shown in fig. 4.2.

4.3 Uncertainty modelling

Considering a multi-input multi-output (MIMO) system, with $\underline{G}_o(s)$ the nominal transfer function matrix and $\underline{G}(s)$ the true transfer function matrix. The uncertainty describing the difference between the true and nominal plants can be modelled in one of many possible ways. The most popular models used are the,

additive model,

$$\underline{G}(s) = \underline{G}_o(s) + \underline{\Delta}_a(s) \quad 4.3.1$$

input multiplicative model,

$$\underline{G}(s) = \underline{G}_o(s) \times [\underline{I} + \underline{\Delta}_i(s)] \quad 4.3.2$$

and the output multiplicative model,

$$\underline{G}(s) = [\underline{I} + \underline{\Delta}_o(s)] \times \underline{G}_o(s) \quad 4.3.3$$

The multiplicative model from equation 4.3.2 gives a relative, rather than absolute uncertainty magnitude as is shown in the following equation,

$$\begin{aligned} \|\underline{G} - \underline{G}_o\|_\infty &= \|\underline{G}_o \underline{\Delta}_i\|_\infty \\ &\leq \|\underline{G}_o\|_\infty \times \|\underline{\Delta}_i\|_\infty \end{aligned} \quad 4.3.4$$

as opposed to the additive model from 4.3.1 which gives an absolute uncertainty magnitude,

$$\|\underline{G} - \underline{G}_o\|_\infty = \|\underline{\Delta}_a\|_\infty \quad 4.3.5$$

Equations 4.3.1 and 4.3.2 with a controller introduced in the feedback path can be represented as shown in figure 4.4(a) and 4.4(b) respectively.

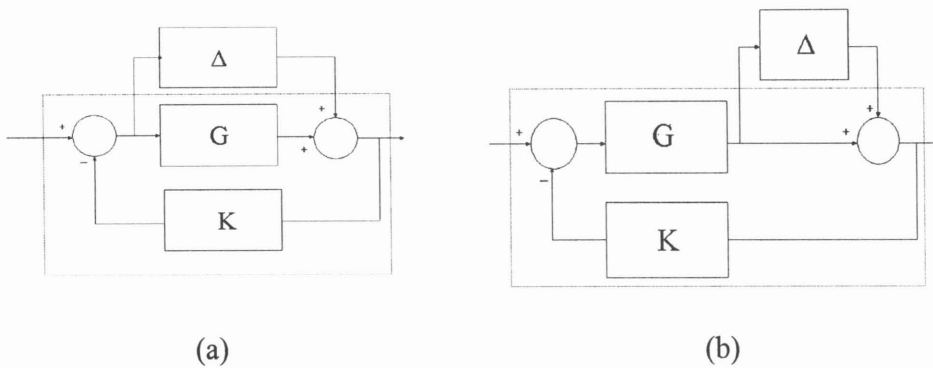


Figure 4.4: (a) additive uncertainty model; (b) multiplicative uncertainty model

If the blocks G and Δ in figure 4.4(a) are SISO blocks with additive uncertainty and the objective is to introduce a controller K in the feedback path. The controller K , must be designed such that robust stability is guaranteed for all uncertainty (Δ).

Equating the section enclosed by the dashed box in figure 4.4(a), to P in figure 4.2, this can be formulated as an H_∞ problem as follows,

$$\left\| K(1 + G_o K)^{-1} \Delta_a \right\|_\infty < 1 \quad \forall \omega \quad 4.3.6$$

If it is possible to place an upper bound on the magnitude of Δ_a with a known function, $B_a(\omega)$, such that,

$$\max \left| \Delta_a(j\omega) \right| \leq B_a(\omega) \quad \forall \omega \quad 4.3.7$$

the following result is obtained.

$$\left| K(j\omega)(I + G_o(j\omega)K(j\omega))^{-1} \right| < \frac{1}{B_a(\omega)} \quad \forall \omega \quad 4.3.8$$

$$\text{i.e.} \quad \left\| K(I + G_o K)^{-1} B_a \right\|_\infty < 1$$

This is a sufficient condition for robust stability of the closed loop in the presence of norm bounded uncertainty (Rao, 1998a).

In the case of multiplicative uncertainty we have the following,

$$\left\| G_o K(I + G_o K)^{-1} B_m \right\|_\infty < 1 \quad 4.3.9$$

with $B_m(\omega)$ being the function used to place an upper bound on the multiplicative uncertainty. Equations 4.3.8 and 4.3.9 indicate that by proper choice of controller $K(s)$, the functions defined on the left of the inequality may be shaped to be smaller

than their respective bounds. This is therefore a guarantee of robust stability of the loop in the presence of uncertainty. If for example disturbance attenuation is the desired criterion for the design of $K(s)$, with the sensitivity function $S = (I+GK)^{-1} \leq W_1(\omega)$, with $W_1(\omega)$ some chosen specification, we can write the following,

$$\left| (I + GK)^{-1} \right| \leq W_1 \quad 4.3.10$$

or using the arguments presented in equation 4.2.6,

$$\left\| (I + GK)^{-1} W_1^{-1} \right\|_\infty \leq 1 \quad 4.3.11$$

A similar argument can be presented for the closed loop transfer function, $T(j\omega)$, as follows. If $W_2(\omega)$ is chosen as the upper bound on $T(j\omega)$ we have the following,

$$\left\| GK(I + GK)^{-1} W_2^{-1} \right\|_\infty \leq 1 \quad 4.3.12$$

These can be incorporated into a mixed sensitivity problem as follows (Maciejowski, 1988),

$$\left\| \begin{matrix} SW_1 \\ TW_2 \end{matrix} \right\|_\infty \leq 1 \quad 4.3.13$$

4.4 Selecting weighting functions

The mixed sensitivity formulation of equation 4.3.13 yields a unique problem in that the synthesized controller contains amongst its zeros, the open loop stable poles of the plant. This results in the poorly damped mode being unobservable at the chosen plant output, with no improvement in damping. Klein *et al* (1994) have exploited a property of the H_∞ algorithm to overcome this problem. The algorithm produces a

controller whose zeros consist of the open loop stable poles of the plant and whose poles contain the poles of $W_1(s)$. The function $W_1(s)$ may therefore be chosen such that, included in its poles are the critical poles of the plant. $W_2(s)$ may be chosen to satisfy the closed loop performance requirements. Klein *et al* (1994) have shown that the specification on closed loop performance can be chosen as a simple high pass filter to achieve the minimisation of the closed loop norm. The problem with this approach is the inability to directly specify the amount of damping improvement desired.

4.5 The standard H_∞ problem

The following discussion follows the presentation in Maciejowski (1988). For the block diagram of the generalised plant in fig 4.5, the 'input' (w), is a vector of all the signals entering the system, 'error' (z) is a vector of all the signals required to characterise the behaviour of the closed loop system. The vector of control signals is represented by ' u ', and ' y ' is the vector of measured outputs. Some elements of ' w ' and ' z ' can be connections to uncertainty blocks as described above.

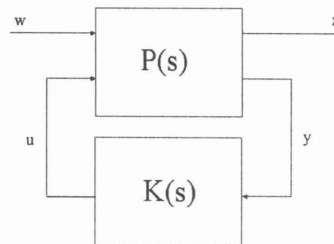


Figure 4.5: Generalised plant model

If $P(s)$ is partitioned as follows,

$$P(s) = \begin{bmatrix} P_{11}(s) & P_{12}(s) \\ P_{21}(s) & P_{22}(s) \end{bmatrix} \quad 4.5.1$$

we can write,

$$z = P_{11}w + P_{12}u \quad \text{and} \quad y = P_{21}w + P_{22}u \quad 4.5.2$$

Eliminating u and y by using $u=Ky$, where K is a feedback controller we have,

$$z = [P_{11} + P_{12}K(I + P_{22}K)^{-1}P_{21}]w \quad 4.5.3$$

with

$$F_l(P, K) = [P_{11} + P_{12}K(I + P_{22}K)^{-1}P_{21}] \quad 4.5.4$$

The standard problem becomes: Find a stabilising controller $K(s)$ such that,

$$\|F_l(P, K)\|_\infty < \gamma \quad 4.5.5$$

or

$$\|\gamma^{-1}F_l(P, K)\|_\infty < 1 \quad 4.5.6$$

for some chosen γ , where $F_l(P, K)$ is a linear fractional mapping, as described by equation 4.5.4, with the subscript 'l' denoting 'lower'. If the feedback path containing K had been drawn above P , an upper transformation would be needed (Maciejowski, 1988). The variable ' γ ' can be optimised iteratively to maximize system robustness to satisfy equation 4.5.6.

In terms of the mixed sensitivity problem formulation, $F_l(P, K)$ becomes,

$$F_l(P, K) = \begin{bmatrix} W_1 S \\ W_2 T \end{bmatrix} \quad 4.5.7$$

The solution to this problem (Glover and Doyle, 1988) is given in Appendix C without derivation but with a brief explanation.

MATLAB provides an implementation of the algorithm in the form of a toolbox (Balas, Doyle and Glover, 1990). This toolbox has been used for the numerical example presented in section 4.6 below.

4.6 H_∞ PSS design example

The design presented in this section follows the ideas formulated by Rao (1998a) for applying H_∞ to PSS design for a SMIB system. A linearized model suffices to represent the SMIB system for the purposes of the small signal design. A nominal model is obtained by linearising the system equations around a chosen nominal operating point. The modelling and system data are given in the Appendices A and B.1, with the linearised model obtained from Kundur (1994). The uncertainty is identified as the deviation in the plant frequency response from the nominal response obtained at a chosen operating point.

In a power system, the range of operating conditions may include both stable and unstable systems. Hence the use of the standard H_∞ problem formulation may result in an unstable Δ . This contradicts the assumptions of the small gain condition (Rao, 1998a; p 32). A modification (Rao, 1998a) is therefore required to adequately define the uncertainty without the above-mentioned violation.

If ΔT_m is assumed to be zero, inspection of the block diagram of the SMIB system (Kundur, 1994), illustrates that the model variation can only be attributed to changes in ΔT_e . The two contributors to changes in ΔT_e , are changes in rotor position ($\Delta\delta$), and changes in the field excitation signal (ΔE_{fd}). Identifying the uncertainties and representing them with upper bounds in the block diagram, results in figure 4.6 shown below.

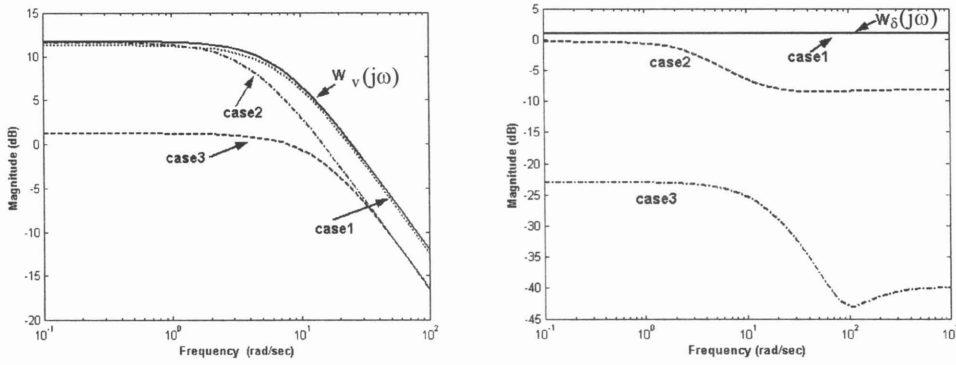


Figure 4.7: Magnitude plots of uncertainty transfer functions

$$W_v = \frac{0.2397 * (s + 111.4024)}{(s + 6.7073)}$$

$$W_\delta = \frac{(0.184 * s + 1.1254)}{(0.1639 * s + 1)}$$

The objective is to design a feedback controller (PSS), to minimize the infinity norm of the closed loop transfer function, $T_{\Delta\omega/Vref}(s)$, and guarantee robust stability with improved system damping for all operating conditions. The weighting function used in the algorithm to minimize the closed loop norm was chosen to have the characteristics of a high pass filter. A Bode magnitude plot of the weighting function is shown in figure 4.9 together with the plant behaviour.

The H_∞ optimal PSS is synthesized using MATLAB's Robust Control Toolbox. The H_∞ algorithm produces controllers of unnecessarily high order. The Bode plot of the resulting controller is shown in figure 4.8. A typical lead type characteristic is demonstrated. The washout term is not included in the PSS transfer function shown in the Bode plot of figure 4.8. The washout term is not part of the synthesized controller and is added as a supplementary term.

Figure 4.9 shows the magnitude plot of all three plant cases with and without the controller, compared with the weighting function. It is clearly visible in figure 4.9(b) that the controller minimizes the magnitude peak, of $P(s)=T_{\Delta\omega/Vref}(s)$, at the oscillatory frequencies.

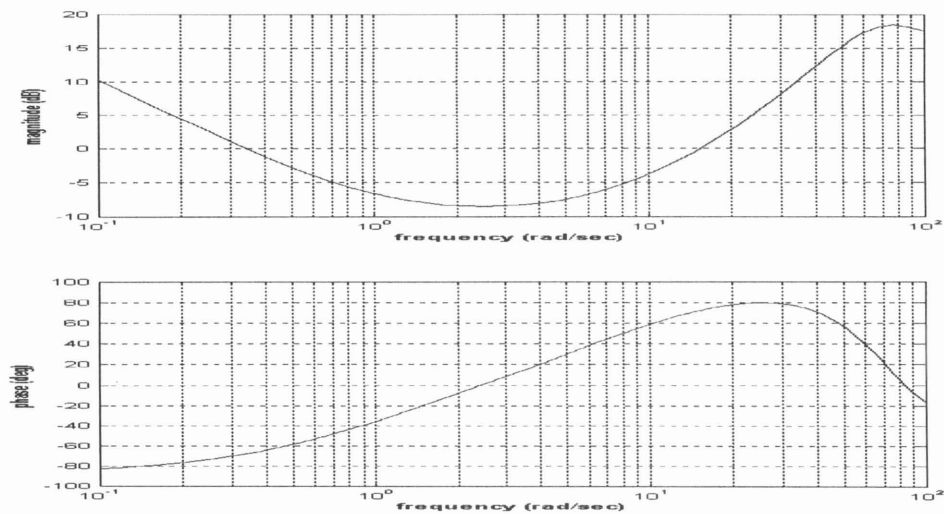


Figure 4.8: Bode plot of the H_∞ PSS

The controller performance in the presence of small disturbances at the AVR reference input is illustrated in figure 4.10. The large disturbance response is illustrated in figure 4.11.

Rao (1998a), highlights that the closed loop norm achieved was greater than one. The same result was obtained for this example. This is an inherent shortcoming of H_∞ optimisation due to its conservativeness, as observed in figure 4.3, in assessing system robustness.

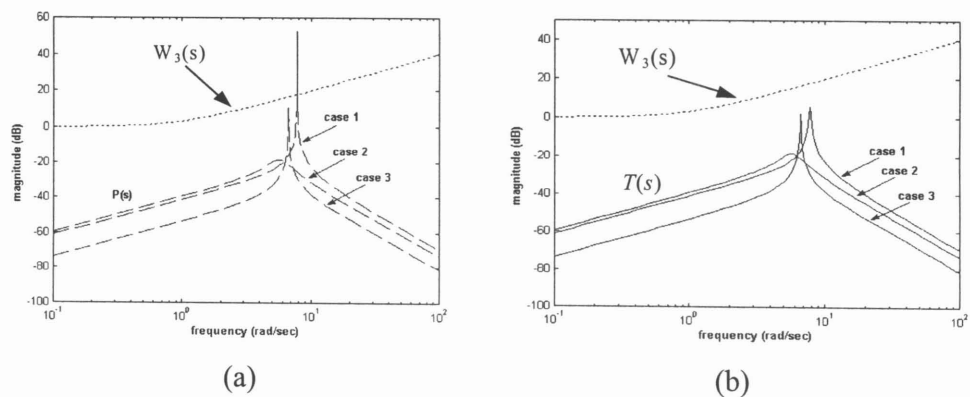


Figure 4.9: (a) Magnitude plot of the open loop plant $P(s)$ and (b) the closed loop $T(s)$

-- no controller — with H_∞ controller weighting function, $W_3(s)$

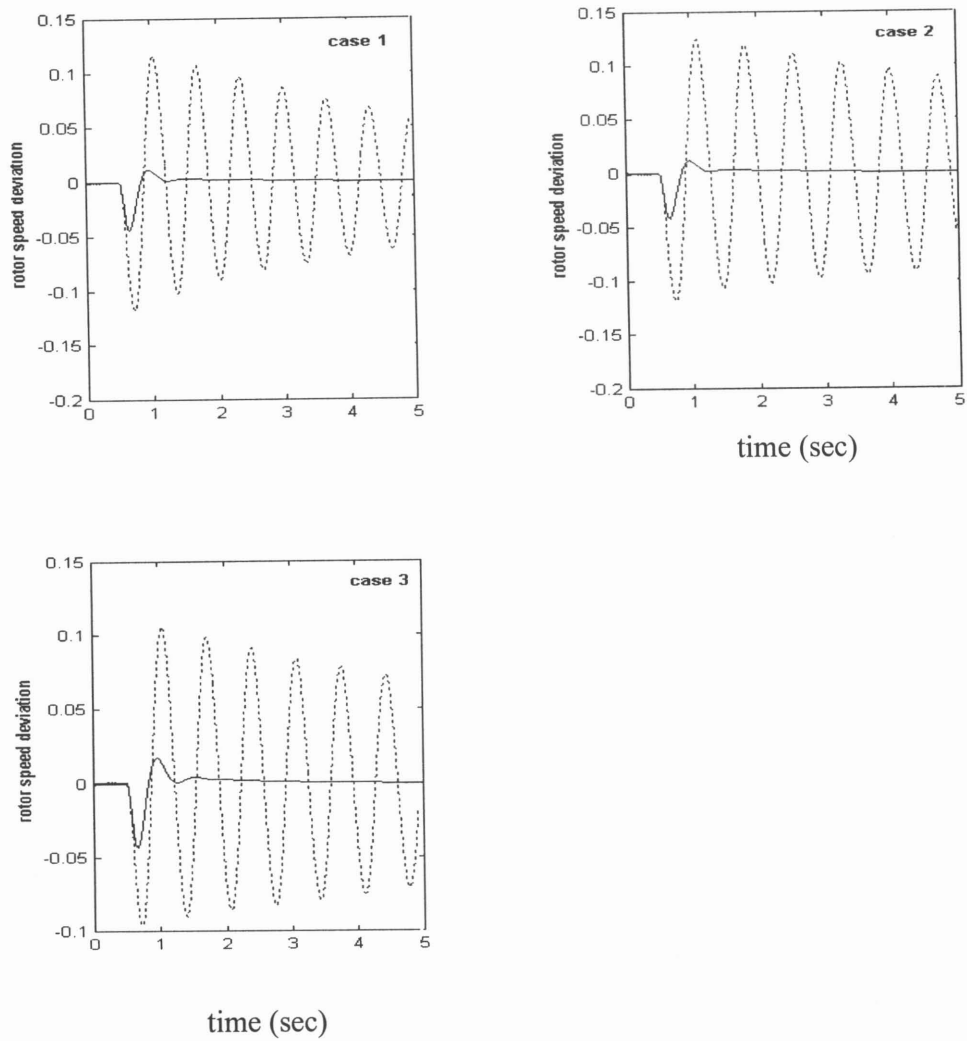


Figure 4.10: Closed loop system response to a 5% step disturbance at the AVR reference input for 100 ms
..... no controller '—' H_{∞} PSS

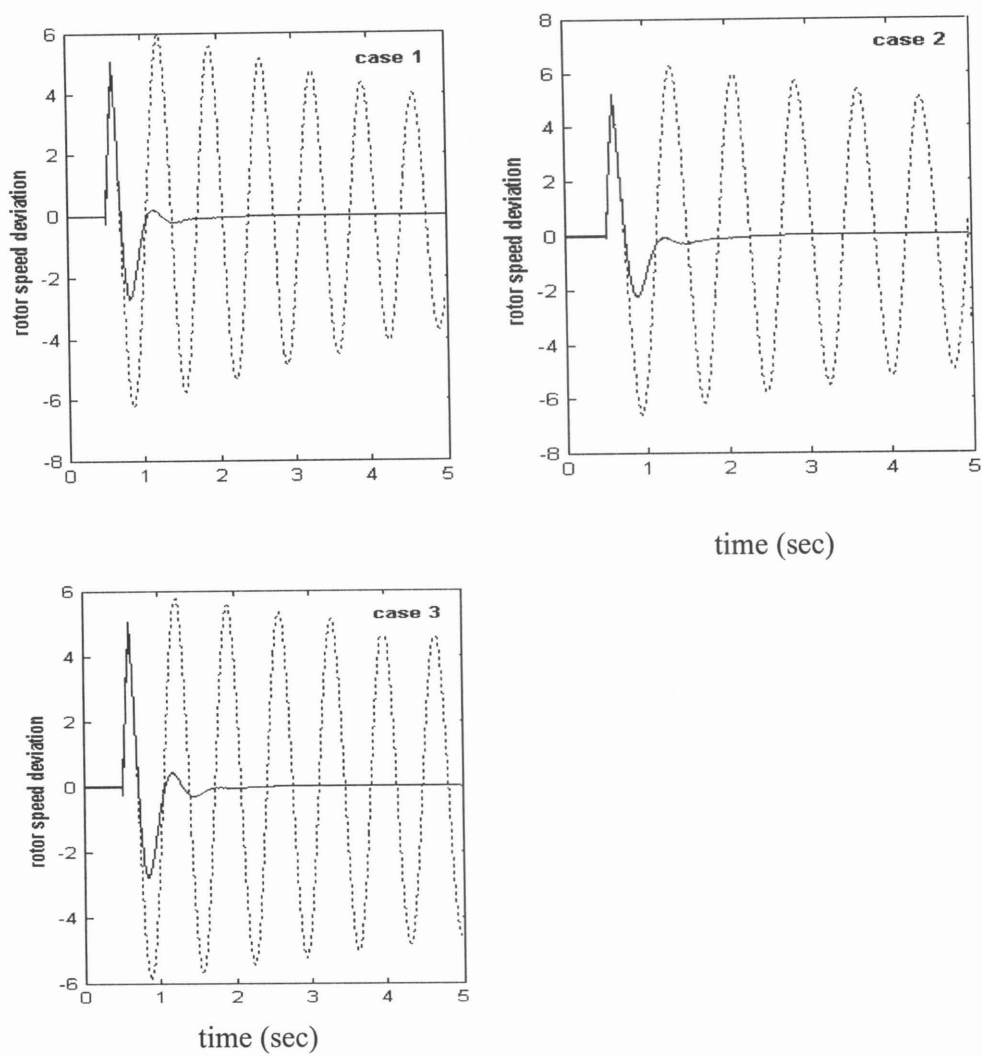


Figure 4.11: Closed loop system response to a three phase fault at the infinite bus for 100 ms
..... no controller '—' H_{∞} PSS

4.7 Extending the range of operating conditions

To find a controller for an extended range of operating conditions requires following the steps identical to those presented in section 4.6. Figure 4.12 illustrates bode magnitude plots of the uncertainty transfer functions for the operating conditions of table 4.2 (Boje *et al*, 2001).

P	Q	Xe	comment
1.0	0.2	0.2	nominal
1.0	-0.2	0.3	leading p.f
1.0	0.5	0.3	lagging p.f
0.9	0.3	0.65	nominal
0.05	0.0	1.08	light load
0.5	-0.2255	1.08	0.9 pf lead
0.05	0.0	0.15	light load
0.1	0.0	0.15	10% load
0.3	0.0	1.08	30% load
0.7	0.3884	1.08	0.85 pf lag
0.9	0.4993	0.615	0.85 pf lag
0.9	-0.4059	0.15	0.9 pf lead

Table 4.2: Extended range of operating conditions.

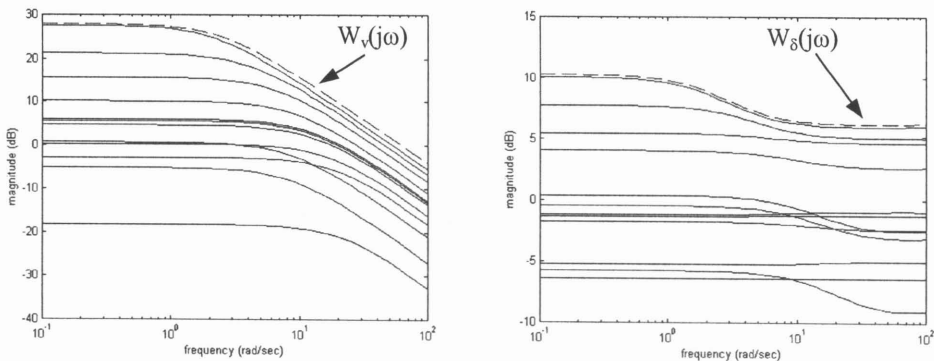


Figure 4.12: Magnitude plots of uncertainty transfer functions for the extended operating range

$$W_v = \frac{25}{(0.4 * s + 1)}$$

$$W_\delta = \frac{1.025 * (0.04s^2 + 4s + 13)}{(0.02s^2 + 2s + 4.2)}$$

It is clearly visible that the uncertainty region has increased and the required upper bounds have become larger if the nominal operating condition remains unchanged. Rao (1998a, p 36), outlines a design of a controller encompassing an extended range of operating conditions. H_∞ fails to generate a controller that provides robust stability for the extended range of operating conditions. It is also shown that most plants in the given plant still remain inadequately damped in the closed loop.

4.8 Summary and conclusions

H_∞ optimisation has been applied over a restricted range of operating conditions to the design of a damping controller for a SMIB system. The controller is observed to possess adequate robustness properties for the chosen range of operating conditions. The key consideration for the design is the choice of the weighting functions.

The designer has no control once the synthesis procedure is set in motion. This is due to the automated nature of the solution algorithm. H_∞ optimal control is seen to be efficient at generating robust controllers albeit of unnecessarily high order.

The inherent conservativeness in H_∞ optimal control can be reduced by the technique known as μ (μ) synthesis. This technique makes use of the quantity known as the '*structured singular value*' (SSV- μ). The SSV is a matrix function that provides a generalization of the largest singular value ($\bar{\sigma}$), (Djukanovic, Khammash and Vittal, 1998). The definition of ' μ ' for a complex matrix ' M ', is the smallest structured perturbation Δ , (measured in terms of $\bar{\sigma}(\Delta)$), that makes $\det(I - M\Delta) = 0$. The SSV is dependent on the complex matrix M and the structure of the uncertainty ' Δ ' and can be thought of as lying between the spectral radius and the *maximum principal gain* of M . The problem definition for ' μ ' synthesis thus becomes one of finding an upper bound for the SSV of the matrix M while simultaneously attempting to design a stabilising controller K . This results in a non-convex problem (Rao, 1998a,b) and solutions are difficult to find. This approach was not investigated as an application to controller design in this thesis.

CHAPTER 5

QFT applied to PSS design

5.1 Introduction

This chapter outlines the design for robust damping controllers (PSS), based on Quantitative Feedback Theory (QFT) as applied to both the SMIB and multi-machine cases.

Application of the QFT design philosophy has recently become widespread in the design of damping controllers for power systems (Sedigh and Alizadeh, 1994; Rao, 1998a; Boje, Nwokah and Jennings, 1999; Boje and Jennings, 2001; Rao and Boje, 2001; Kelemen and Akhrif, 2002). The conventional QFT approach deals with shaping of the loop transmission, $\forall P \in \{P\}$, to satisfy bounds at every frequency placed on the closed loop system functions, eg: output sensitivity function.

An introduction to QFT for an arbitrary SISO case is provided before practical application to a power system is illustrated. A controller is designed for the SMIB case with the same restricted range of operating conditions used in Chapters Three and Four. The controller design for the SMIB case is then undertaken for an extended range of operating conditions. The objective is to illustrate the ease with which QFT handles templates of varying sizes and shapes as opposed to H_∞ . Both these designs are treated as SISO type designs with the AVR and governor loops closed. The final design example applies QFT to the more interesting and challenging problem of multi-machine stabiliser design.

The first SMIB design proceeds as a standard SISO design for a SMIB case. The range of operating conditions is then extended and the PSS is designed using the ideas presented by Boje and Jennings (2001).

The multi-machine PSS design is undertaken to encompass four operating conditions, one being that of a generator outage scenario. The structured singular value is introduced as an adequate system robust stability measure. It is shown to be useful in obtaining the stability boundaries required in QFT controller designs for multi-machine networks. The design follows on a recent paper by Rao and Boje (2001) who have applied QFT to multi-machine PSS design.

A brief discussion of the multi-machine study system is also given to outline the structure and define the problem to be solved. The study system is obtained from Kundur (1994) and has been successfully used to study the problem of inter-area mode oscillations (Klein *et al*, 1992).

5.2 QFT tracking design for SISO systems

Consider the generalised two-degree of freedom plant structure shown in figure 5.1.

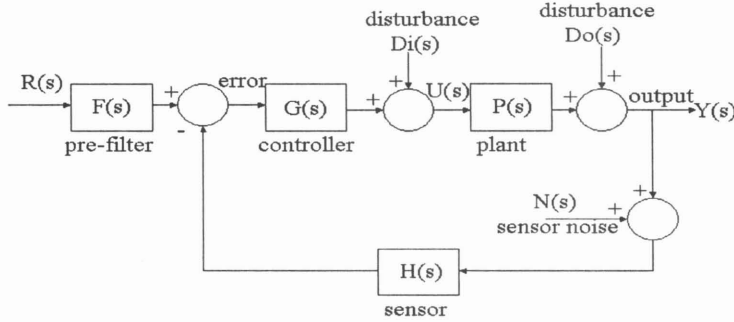


Figure 5.1: 2 DOF structure

If the plant has significant uncertainty and belongs to a set of plants, $P(s) \in \{P\}$, containing both stable and unstable cases, the output $Y(s)$ belongs to a set of outputs $\{Y\}$ for any given $R(s)$. The closed loop tracking transfer function is given by,

$$T_{Y/R}(s) = \frac{FGP}{1 + GPH} = \frac{F}{H} \frac{L}{1 + L} \quad 5.2.1$$

for $L = GP$.

The objective is to design $G(s)$ such that variations in the plant cause $Y(s)$ to lie only within a defined region for a given input $R(s)$. This is accomplished in the QFT framework by placing magnitude constraints on the closed loop transfer function as in equation 5.2.2 below. If the function $F(s)$ is other than unity, it is typically designed after $G(s)$ to ensure that $Y(s)$ achieves the desired tracking of $R(s)$.

$$b(\omega)_{dB} \leq |T(j\omega)|_{dB} \leq a(\omega)_{dB} \quad \forall P, \omega \quad 5.2.2$$

Figure 5.2 shows tracking boundary specifications for an arbitrary example system in the frequency domain with its translation onto the Nichols chart. This is done

using the *sisobnds*(7,...) command from MATLAB's 'QFT' toolbox (Borghesani, Chait and Yaniv, 1994). The area defined below the solid contours in figure 5.2(b) is used as an exclusion region for the design of G at each frequency. The nominal loop transmission $L_0(j\omega) = P_0(j\omega)G(j\omega)$ is manually shaped to simultaneously satisfy the boundary constraint at all frequencies for every plant case in the plant set. This guarantees robustness of the designed controller.

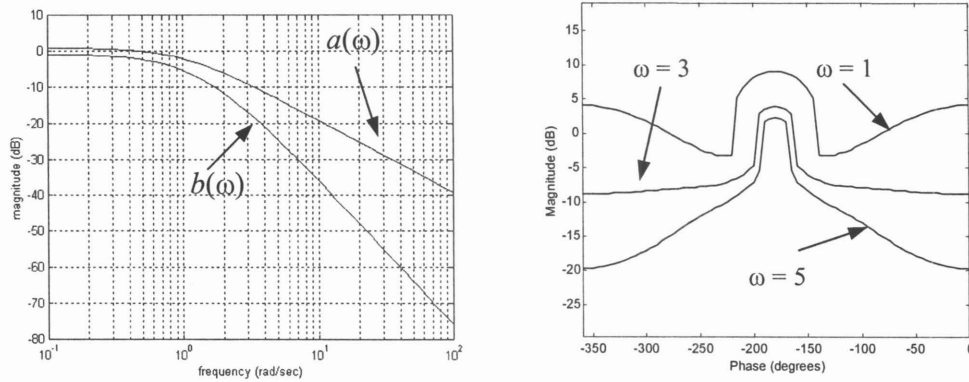


Figure 5.2: Frequency domain boundary specifications with translation onto the Nichols chart

Similar arguments can be presented for other system functions, for example the output sensitivity function. Robust stability boundaries may also be added if performance specification is not the only concern.

The ideas in SISO QFT are now illustrated with the simple example below (Boje, 2001). Consider a plant given by the following,

$$P = \frac{k}{s} \quad \text{with} \quad k \in [1, 5]$$

Design a feedback controller $G(s)$ to achieve the following,

$$b1: \left| \frac{1}{1+L} \right| \leq -20dB \quad \forall \quad \omega \leq 0.5$$

$$b2: \left| \frac{1}{1+L} \right| \leq 3dB \quad \forall \quad \omega$$

These are magnitude specifications for the output sensitivity function. Figure 5.3(a) shows the boundaries on the Nichols chart, plotted together with the nominal plant chosen for $k = 1$. The nominal plant can be chosen as any one of the possible plant cases in the plant set. The boundaries are plotted using the `sisobnds(2,...)` command from the toolbox. Figure 5.3(b) shows the nominal loop after being shaped, using the 'LPSHAPE' command from the toolbox, to satisfy the boundary constraints. The controller is given by the change in gain and phase added to the nominal plant to satisfy the boundary constraints.

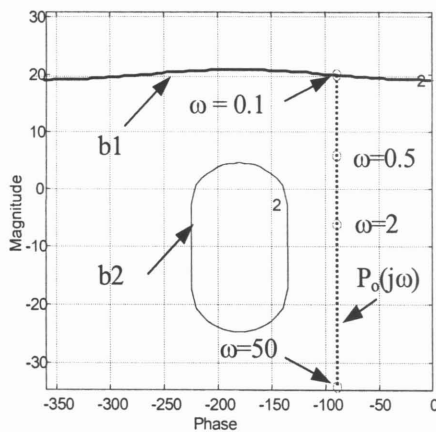
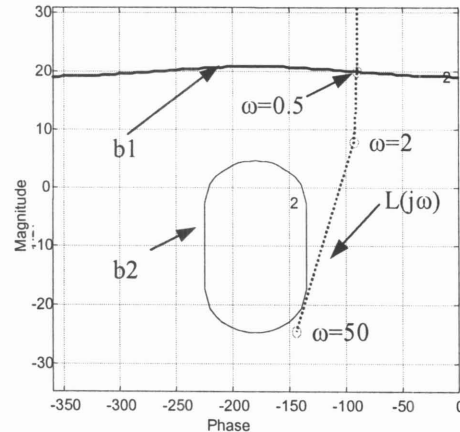


Figure 5.3: (a) Nominal plant



(b) Nominal plant with controller

A controller satisfying the above constraints is found with the graphical user interface (GUI) in the toolbox and is given by,

$$G = \frac{5}{s/36.8 + 1}$$

A controller that satisfies the design specifications exactly at each frequency and minimises the high frequency gain, for a given excess of poles over zeros, may be regarded as 'optimal' in the sense of minimising the high frequency noise. Practical

controllers are low order and therefore probably will not be optimal in the above sense.

The example serves to illustrate the use of QFT and its ease of application in the SISO case. Figure 5.4 shows Bode magnitude plots of the output sensitivity function for all plant cases satisfying the specifications used for the design of the controller.

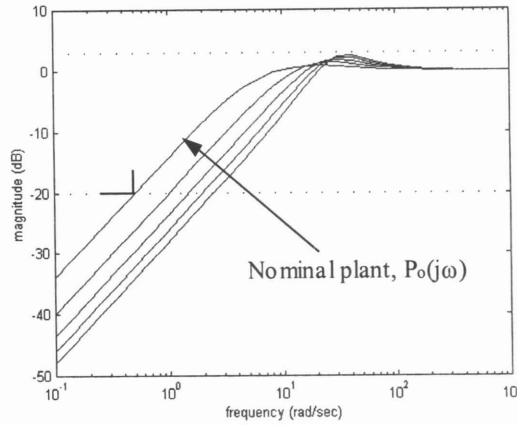


Figure 5.4: '—' output sensitivity function, '...' design specifications

5.3 Extension to the multi-variable case

5.3.1 Diagonal controller design

This section extends the design methodology of the first section to multi-variable systems. This only serves to introduce some basic ideas on the vastly diverse topic of multi-variable QFT design. A more in-depth discussion can be found in Horowitz (1992), Boje (2001) and Yaniv (1999). The formulation outlined accomplishes the design of \mathbf{G} one element at a time and uses back substitution of the designed controllers to ease over-design in the subsequent loops. This is not a sequential loop closure approach as the specifications are used to over-bound the unknown elements as will be illustrated. The output sensitivity function will be used to illustrate an approach in MIMO system design (Boje, 2001). The controller structure is assumed to be diagonal in nature. Let $\mathbf{P}(s)$ in figure 5.1 be an $m \times m$ matrix in general, $\mathbf{P}(s) \in \{\mathbf{P}\}$, but be described by a 2×2 case as follows for illustration,

$$P(s) = \begin{pmatrix} p_{11}(s) & p_{12}(s) \\ p_{21}(s) & p_{22}(s) \end{pmatrix} \quad 5.3.1.1$$

with the following assumed properties

- 1) P is diagonally dominant such that $p_{11}p_{22} > p_{12}p_{21}$ at frequencies of interest
- 2) P is square and invertible (to allow inversion required for this formulation)

The above assumptions are added to ease the discussion but are not a necessity. The formulation may proceed without the requirement for the inversion of the plant matrix but is not shown here. Constraint one is added to validate the argument for the assumption of a diagonal controller structure. For plants displaying strong interaction between the diagonal and off-diagonal elements of the plant matrix, assumption one is invalid. Techniques do however exist to design controllers in this case, with the controller comprising a de-coupling element and a diagonal controller (Boje, 2001). The controller G in this formulation is defined as having the following structure,

$$G = \begin{pmatrix} g_1 & 0 \\ 0 & g_2 \end{pmatrix} \quad 5.3.1.2$$

The design objective is identical to that in section 5.2. The output sensitivity transfer function is chosen for the illustration and is given by,

$$T = (I + PG)^{-1} \quad 5.3.1.3$$

Equation 5.3.1.2 can be re-written as follows,

$$(I + PG)T = I \quad 5.3.1.4$$

With $\hat{P} = P^{-1}$ equation 5.3.1.4 becomes,

$$(\hat{P} + G)T = \hat{P} \quad 5.3.1.5$$

Expanding equation 5.3.1.5 into its individual elements gives,

$$\begin{pmatrix} \hat{p}_{11} + g_1 & \hat{p}_{12} \\ \hat{p}_{21} & \hat{p}_{22} + g_2 \end{pmatrix} \begin{pmatrix} t_{11} & t_{12} \\ t_{21} & t_{22} \end{pmatrix} = \begin{pmatrix} \hat{p}_{11} & \hat{p}_{12} \\ \hat{p}_{21} & \hat{p}_{22} \end{pmatrix} \quad 5.3.1.6$$

Writing the elements of \hat{P} as $\hat{p}_{ij} = 1/q_{ij}$, where the q_{ij} are transfer function elements, equation 5.3.1.6 becomes,

$$\begin{pmatrix} \frac{1}{q_{11}} + g_1 & \frac{1}{q_{12}} \\ \frac{1}{q_{21}} & \frac{1}{q_{22}} + g_2 \end{pmatrix} \begin{pmatrix} t_{11} & t_{12} \\ t_{21} & t_{22} \end{pmatrix} = \begin{pmatrix} \frac{1}{q_{11}} & \frac{1}{q_{12}} \\ \frac{1}{q_{21}} & \frac{1}{q_{22}} \end{pmatrix} \quad 5.3.1.7$$

Multiplying each row of equation 5.3.1.7 by the respective q_{ii} element it becomes,

$$\begin{pmatrix} 1 + q_{11}g_1 & q_{11}/q_{12} \\ q_{22}/q_{21} & 1 + q_{22}g_2 \end{pmatrix} \begin{pmatrix} t_{11} & t_{12} \\ t_{21} & t_{22} \end{pmatrix} = \begin{pmatrix} 1 & q_{11}/q_{12} \\ q_{22}/q_{21} & 1 \end{pmatrix} \quad 5.3.1.8$$

Solving for the individual rows with, $l_i = q_{ii}g_i$, equation 5.3.1.8 gives for row one,

$$t_{11} = \frac{1}{1 + l_1} \left(1 - t_{21} \frac{q_{11}}{q_{12}} \right) \quad 5.3.1.9$$

and

$$t_{12} = \frac{1}{1 + l_1} \left(\frac{q_{11}}{q_{12}} (1 - t_{22}) \right) \quad 5.3.1.10$$

Equations 5.3.1.9 and 5.3.1.10 give two design equations for the first controller element, g_{11} , but still contain the unknown t_{ij} elements preventing a solution for the controller. Over-bounding the unknown elements with their respective specifications and using the Schwartz inequality to generate the maximum boundary specification circumvents the problem. If the magnitude of $t_{ij}(j\omega) \leq a_{ij}(\omega)$ for all ω and P , each unknown element $t_{ij}(j\omega)$ may be replaced by a known $a_{ij}(\omega)$ in the design of the first loop as follows,

$$\left| \frac{1}{1+L_1} \right| \leq \frac{a_{11}}{\max \left| 1 + a_{21} \left\| \frac{q_{11}}{q_{12}} \right\| \right|} \quad 5.3.1.11$$

$$\left| \frac{1}{1+L_1} \right| \leq \frac{a_{12}}{\max \left\| \frac{q_{11}}{q_{12}} \right\| (a_{22} + 1)} \quad 5.3.1.12$$

The design for g_1 may now proceed as for a SISO system. After the design of g_1 is accomplished, the unknown elements for the design of the second loop may be removed from equation 5.3.1.6 by using Gauss-Jordan elimination in the following way. The first row is replaced by,

$$R_1 \rightarrow R_1 \times \frac{\hat{p}_{21}}{\hat{p}_{11} + g_1} \quad 5.3.1.13$$

The second row is then replaced by,

$$R_2 \rightarrow R_2 - R_1 \quad 5.3.1.14$$

Written explicitly, equation 5.3.1.14 becomes,

$$\begin{pmatrix} 0 & \hat{p}_{22} - \frac{\hat{p}_{21}}{\hat{p}_{11} + g_1} \hat{p}_{12} + g_2 \end{pmatrix} T =$$

$$\begin{pmatrix} \hat{p}_{21} - \frac{\hat{p}_{21}}{\hat{p}_{11} + g_1} \hat{p}_{11} & \hat{p}_{22} - \frac{\hat{p}_{21}}{\hat{p}_{11} + g_1} \hat{p}_{12} \end{pmatrix}$$
5.3.1.15

Replacing the terms not containing g_2 in equation 5.3.1.15 by,

$$\hat{p}_{22}^* = \hat{p}_{22} - \frac{\hat{p}_{21}}{\hat{p}_{11} + g_1} \hat{p}_{12}$$

$$\hat{p}_{21}^* = \hat{p}_{21} - \frac{\hat{p}_{21}}{\hat{p}_{11} + g_1} \hat{p}_{11}$$
5.3.1.15

the familiar SISO formulation emerges,

$$t_{22} = \frac{\hat{p}_{22}^*}{\hat{p}_{22}^* + g_2} = \frac{1}{1 + l_2^*}$$

$$t_{21} = \frac{\hat{p}_{21}^*}{\hat{p}_{22}^* + g_2} = \frac{q_{22}}{q_{21}} \frac{1}{1 + l_2^*}$$
5.3.1.16

where $\hat{p}_{2j}^* = 1/\hat{q}_{2j}^*$. Equation 5.3.1.16 gives two exact design equations for g_2 without the requirement for over-bounding the unknowns. This is true for the last design step of any controller design using this formulation.

The design for reference tracking is marginally more difficult and an example of the first element of the first row, t_{11} , is shown in equation 5.3.1.17. The pre-filter $F(s)$ is chosen to be identity. For a tracking transfer function given by equation 5.3.1.17.

$$T = PGF(I + PG)^{-1}$$
5.3.1.17

The first element of the first row is given by,

$$t_{11} = \frac{l_1}{1+l_1} - \frac{q_{11}}{q_{12}} t_{21} \frac{1}{1+l_1} \quad 5.3.1.18$$

If the requirement is, $b(\omega) < |t_{11}(j\omega)| < a(\omega)$, the specification on t_{11} now needs to be divided between the two terms on the right hand side of equation 5.3.1.18. This is shown graphically in figure 5.5. The design is now ‘split’ into two parts and is shown in equation 5.3.1.19. A closed form solution to calculate the boundaries has been formulated by Boje (2001).

$$\left| \frac{1}{1+l_1} \right| < \delta(\omega) \quad 5.3.1.19$$

$$\underbrace{b(\omega) + \delta(\omega)}_{b'(\omega)} < \left| \frac{l_1}{1+l_1} \right| < \underbrace{a(\omega) - \delta(\omega)}_{a'(\omega)}$$

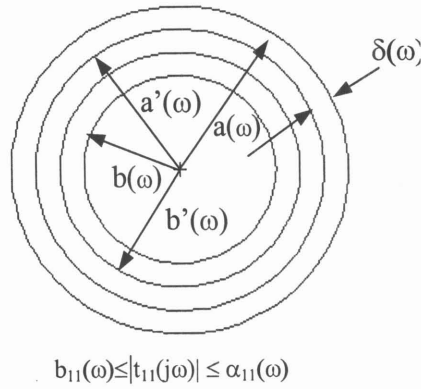


Figure 5.5: Boundary division for
tracking design

5.4 SMIB PSS design example using QFT

5.4.1 Design for a restricted range of operating conditions

This section outlines the SISO QFT method applied to SMIB PSS design. The machine model used here is the same as that used in all previous examples presented. The machine model assumes the presence of an AVR but no governor controls. The restricted range of operating conditions as used in Chapters Three and Four is once again used for the design. In QFT designs the plant is described as a complex number at every frequency, for each plant case. The uncertainty is defined as the deviation in the frequency response for each plant case, with respect to a chosen nominal plant case. The nominal plant case in this example is chosen as Case One in Table 3.1. The open loop plant template can be formed as a set of complex numbers that contains all possible plant behaviours at every frequency considered, thus completely describing the plant uncertainty. The open loop plant characteristics are once again shown in figure 5.6 for ease of reference.

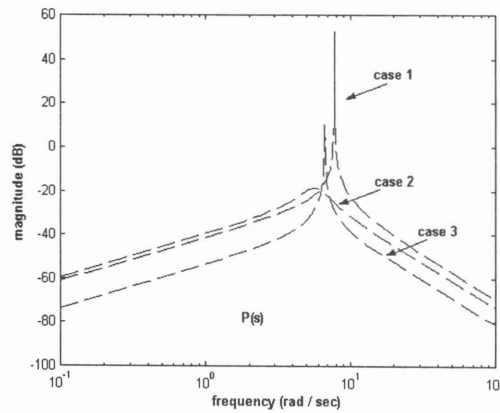


Figure 5.6: Open loop plant characteristics ($T_{\Delta\omega_r / V_{ref}}$)

The design specifications (2) and (3) given below are chosen based on the open loop plant behaviour and follow on the ideas presented by Boje *et al* (1999). The specifications may be modified to suit practical design needs.

- 1) Stabilize the unstable plant cases

- 2) $\left| \frac{1}{1+l_{pss}} \right| \leq 3dB \quad \forall P, \omega$ to ensure robust stability
- 3) $\left| \frac{P}{1+l_{pss}} \right| \leq -10dB \quad \forall P, \omega$ to provide improvement in the closed loop damping

The element P , in specification three above represents the open loop plant with the AVR loop closed. The specification of $-10dB$ for closed loop performance improvement around the modal frequency was chosen to minimize the magnitude peaks displayed by the open loop plant. This example is illustrative and the specifications may not be realistic in practice. Practical design specifications are normally defined as a client requirement. The loop transmission described in specification three above is $l_{pss} = Pg_{pss}$, where g_{pss} represents the PSS description. The specifications for the design are translated onto the Nichols chart and the design constraints are shown in Figure 5.7(a), plotted for frequencies around the oscillatory mode of each plant case.

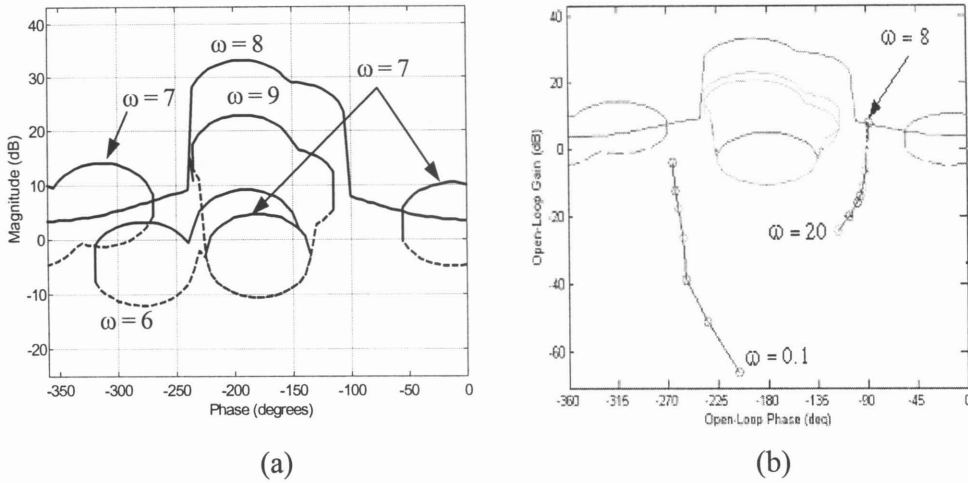


Figure 5.7: (a) Boundary constraints for the SMIB system
(b) nominal plant with the controller added

After shaping the nominal plant to satisfy the boundary constraints, the PSS is read off from the GUI in the normal manner. The nominal plant with the designed controller in place is shown in figure 5.7(b). The PSS that stabilizes and meets the specifications for all three plant cases is given by equation 5.4.1.1.

$$PSS = 1.3 \frac{5s}{(5s+1)} \frac{(0.2842s+1)}{(0.0352s+1)} \quad 5.4.1.1$$

A Bode plot of the resulting PSS, before addition of the washout term, is shown in figure 5.8 below. A lead network once again suffices to meet the requirements for the design. The phase lead added is approximately the same as that added by the conventionally designed PSS of Chapter Three. The H_∞ PSS of Chapter Four adds marginally more phase lead for the same operating conditions. The gain contributions of all the PSS's are approximately the same.

Figure 5.9 shows the Bode magnitude plot of the closed loop system after the addition of the PSS. The closed loop magnitude does not exceed the design specification as expected. The PSS performance for disturbance conditions is assessed using a non-linear simulation in PSCAD/EMTDC and the results are shown in Figures 5.10 and 5.11. Figure 5.10 illustrates the closed loop behaviour for small step changes in the AVR input. Figure 5.11 illustrates the controller performance in the presence of a three-phase fault at the infinite bus.

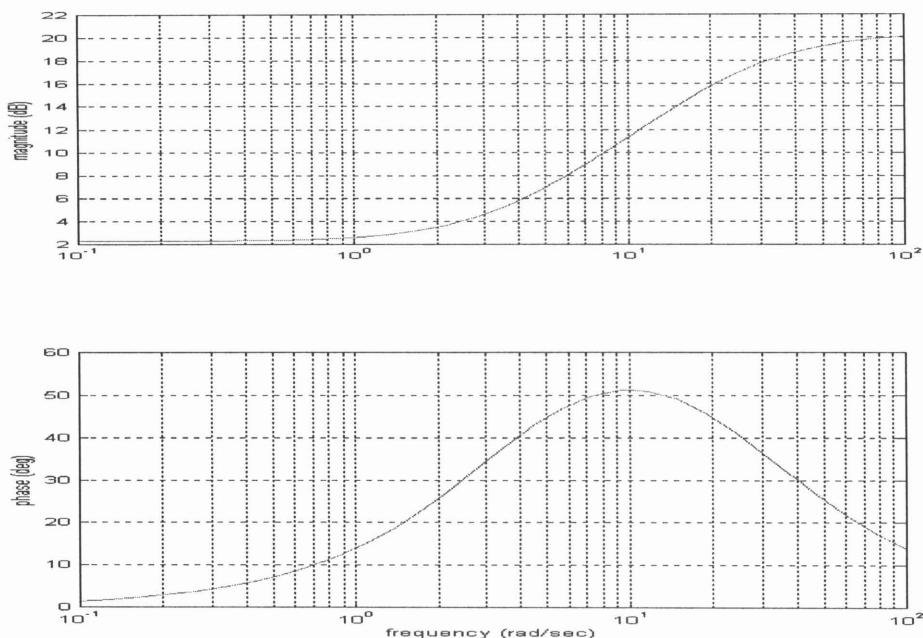


Figure 5.8: Bode plot of the controller

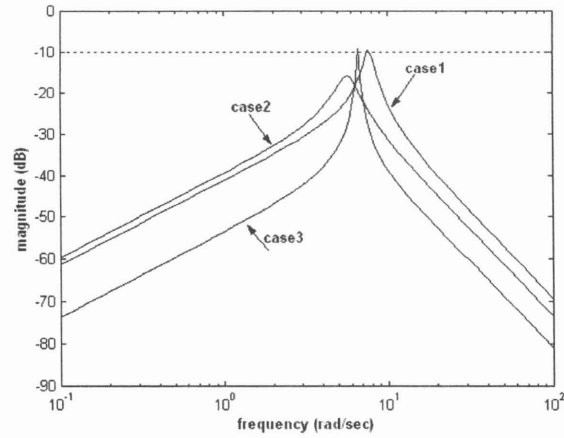


Figure 5.9: — Magnitude plot of the closed loop plant $T(s)$
 Specification on the closed loop performance

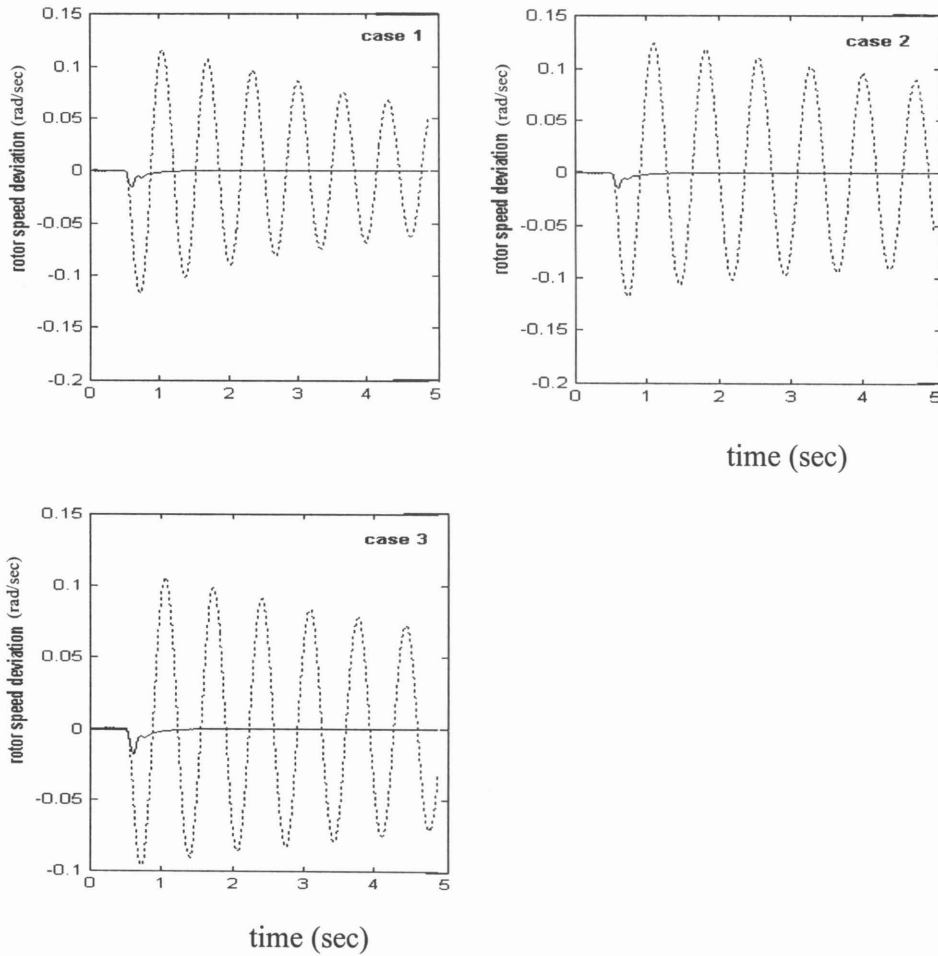


Figure 5.10: Closed loop system response to a 5% step disturbance at the AVR reference input for 100 ms
 no controller — with PSS

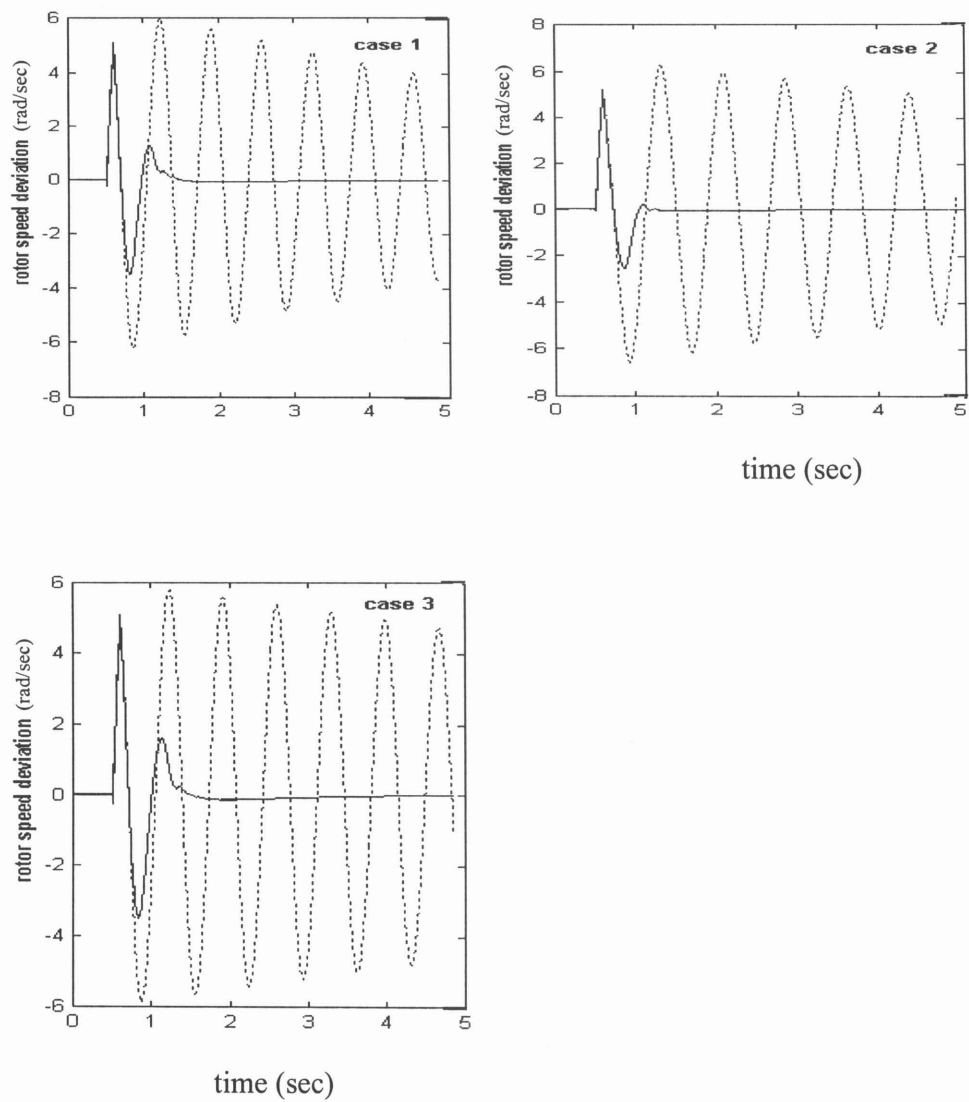


Figure 5.11: Closed loop system response to a three phase fault at the infinite bus for 100 ms

..... no controller — with PSS

5.4.2 Extending the range of operating conditions

Increased bandwidth of the terminal voltage control loop has invalidated the assumption that the speed and voltage control loops are completely de-coupled and can be designed as independent SISO systems (Boje *et al*, 1999). In this example the effect of the PSS on the mechanical and electrical systems will be illustrated. The effect on stability, of both the mechanical and electrical loops after the addition of the PSS will be highlighted. The machine in this example is modelled as a two-input, two-output, third order system and is given in Appendix B.3. The inputs are changes in the mechanical torque and the field excitation signals. The outputs are chosen as the rotor speed deviations and changes in terminal voltage. The AVR and governor controls are provided as external controllers added to the system (Appendix B.3). The speed and voltage controllers are incorporated into the forward path of the system description. In the transfer function description the off-diagonal elements represent the coupling between the electrical and mechanical systems. The range of operating conditions for this example has been extended to show how QFT deals with a large operating range as compared to H_∞ . The range of operating conditions for the design is given in Table 4.2 (Boje *et al*, 2001). The work presented here closely follows the work presented in the above reference.

The machine is described by a third order linearised model and is taken from Kundur (chapter 12, 1994)

The elements of the open loop plant matrix $\underline{P}(s)$ without the controllers in place is given in Appendix A.3. With the speed and voltage controllers in place the closed loop description reduces to,

$$\begin{pmatrix} \Delta\omega_r(s) \\ \Delta V_t(s) \end{pmatrix} = \underline{T}(s) \begin{pmatrix} \Delta T_m(s) \\ \Delta V_{ref}(s) \end{pmatrix} \quad 5.4.2.1$$

With the speed and voltage loops closed the system can be viewed as a SISO system if $\Delta T_m(s)$ is considered to be zero. The PSS is the only element of a feedback controller G given by,

$$G = \begin{pmatrix} 0 & 0 \\ g_{PSS} & 0 \end{pmatrix} \quad 5.4.2.5$$

With the PSS added to the system, the closed loop tracking transfer function becomes,

$$\begin{aligned} T^* &= (I + TG)^{-1}T \\ &= \frac{1}{1 + t_{12}g_{PSS}} \begin{pmatrix} 1 & 0 \\ -t_{22}g_{PSS} & 1 + t_{12}g_{PSS} \end{pmatrix} \begin{pmatrix} t_{11} & t_{12} \\ t_{21} & t_{22} \end{pmatrix} \\ &= \frac{1}{1 + t_{12}g_{PSS}} \begin{pmatrix} t_{11} & t_{12} \\ t_{21}^* & t_{22} \end{pmatrix} \end{aligned} \quad 5.4.2.6$$

where $t_{21}^* = t_{21} + (t_{21}t_{12} - t_{11}t_{22})g_{PSS}$. The element T in equation 5.4.2.6 above represents the closed loop transfer function with the speed and voltage loops closed. Writing the equation for the output speed deviation after the PSS is added to the open loop system as,

$$\Delta\omega(s) = t_{11}(s)\Delta T_m + t_{12}(s)\Delta V_{ref} \quad 5.2.2.7$$

it can be seen that $t_{12}(s)$ represents the effect of changes in ΔV_{ref} on the output speed deviation. It is evident from equation 5.4.2.6 that the overall stability of the system is determined by the stability of the power system stabiliser loop. Boje *et al* (2001) indicate that designing the power system stabiliser loop to be stable will ensure stability of the closed loop system, provided that there is no state that is unstable, being unobservable from the speed measurement and uncontrollable from the AVR input.

For regulation of output disturbances, following the steps similar to that of the tracking objective, the output sensitivity function after the PSS is added becomes,

$$S^* = (I + TG)^{-1}S \quad 5.4.2.8$$

Written explicitly equation 5.4.2.8 is given as,

$$S^* = \frac{1}{1 + t_{12}g_{PSS}} \begin{pmatrix} s_{11} & s_{12} \\ s_{21}^* & s_{22}^* \end{pmatrix} \quad 5.4.2.9$$

with the s_{2j}^* , as follows,

$$\begin{aligned} s_{21}^* &= s_{21} + g_{PSS}(t_{12}s_{21} - t_{22}s_{11}) \\ s_{22}^* &= s_{22} + g_{PSS}(t_{12}s_{22} - t_{22}s_{12}) \end{aligned}$$

It is again evident that stability of the PSS loop is shown to have an impact on the stability of the overall sensitivity function. The design can now commence with the specifications (Boje *et al*, 2001), as follows

1) Stabilise the plant if unstable

$$2) \left| \frac{1}{1 + l_{PSS}} \right| \leq 3_{dB} \quad , \text{ to ensure robust stability}$$

$$3) \left| \frac{t_{11}}{1 + l_{PSS}} \right| \leq (10_{dB} + |t_{11}(j0)|_{dB}) \quad \forall \omega, \text{ to provide damping torque in the speed loop}$$

The range of operating conditions is given in table 4.2. Extending the range of operating conditions only requires increasing the size of the template describing the region of possible plants. This is more straightforward than the H_∞ method which requires bounding the uncertainty. Because of the over-bounding required on the extended uncertainty in H_∞ for this example, a solution to the design problem could not be found. Figure 5.12 shows the open loop magnitude plots of the transfer function matrix elements. The design once again proceeds with plotting the boundaries and shaping a chosen nominal plant loop. An initial ‘guess’ for the controller can be made consisting of only the washout term to include its effect on the overall designed PSS. Figure 5.13 shows the closed loop plant matrix elements with the designed PSS in place. Figure 5.14 and 5.15 illustrate non-linear time domain simulations for small and large disturbances for all operating conditions of

Table 4.2. Figure 5.14 shows the system response to a small change in the AVR reference input, with figure 5.15 showing the system response to a three-phase fault at the infinite bus. The non-linear simulations were carried out in MATLAB. The original software was provided by Rigby (2000). The required changes were made satisfy the specific requirements of the example.

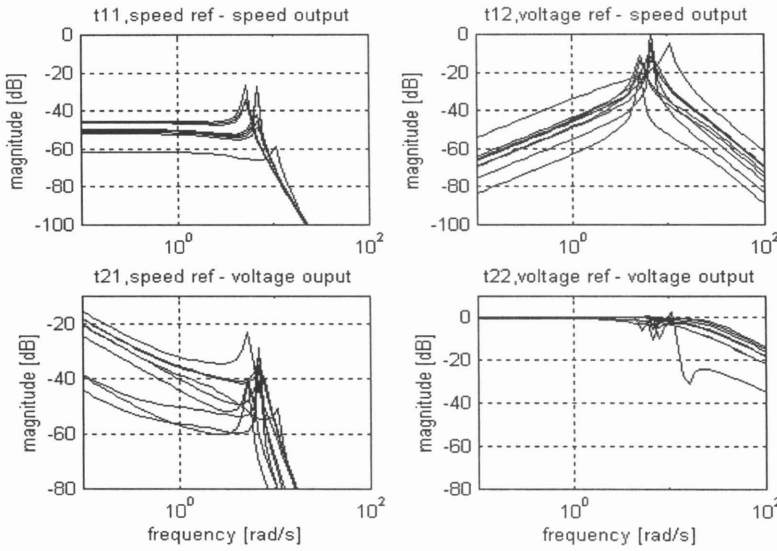


Figure 5.12: Magnitude plots of the open loop transfer function matrix elements

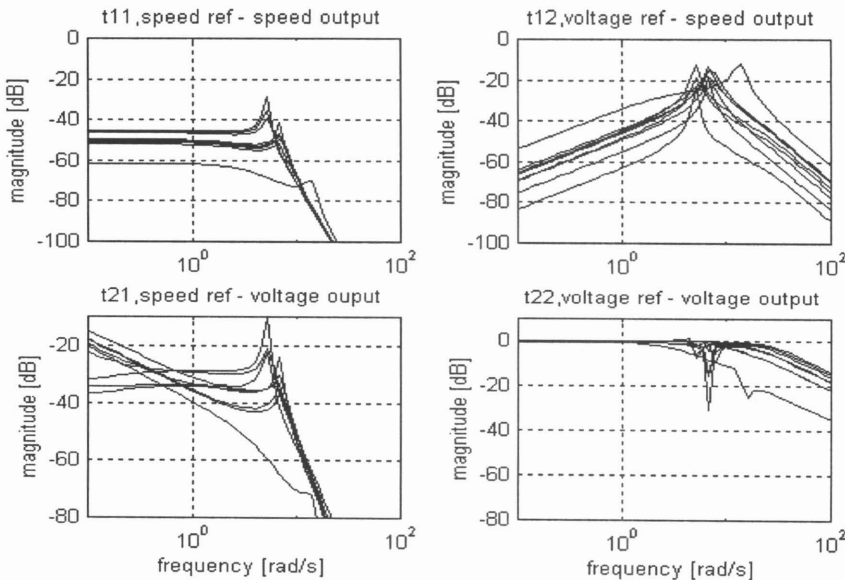


Figure 5.13: Magnitude plots of the closed loop transfer function matrix elements with the PSS added

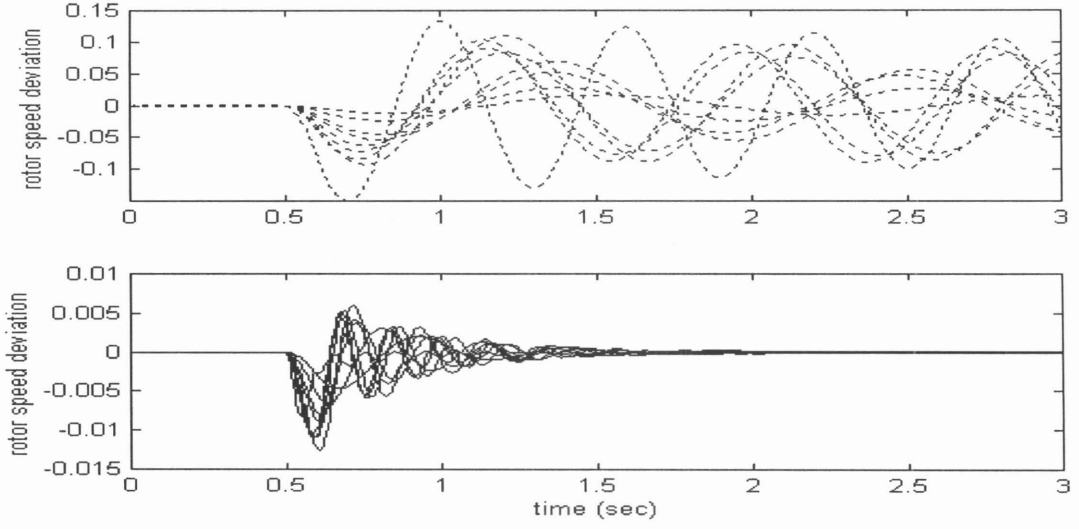


Figure 5.14: System responses to a 5% step disturbance at the AVR input for 100 ms ($T_{\Delta\omega_r/V_{ref}}$)

.... no controller — with PSS

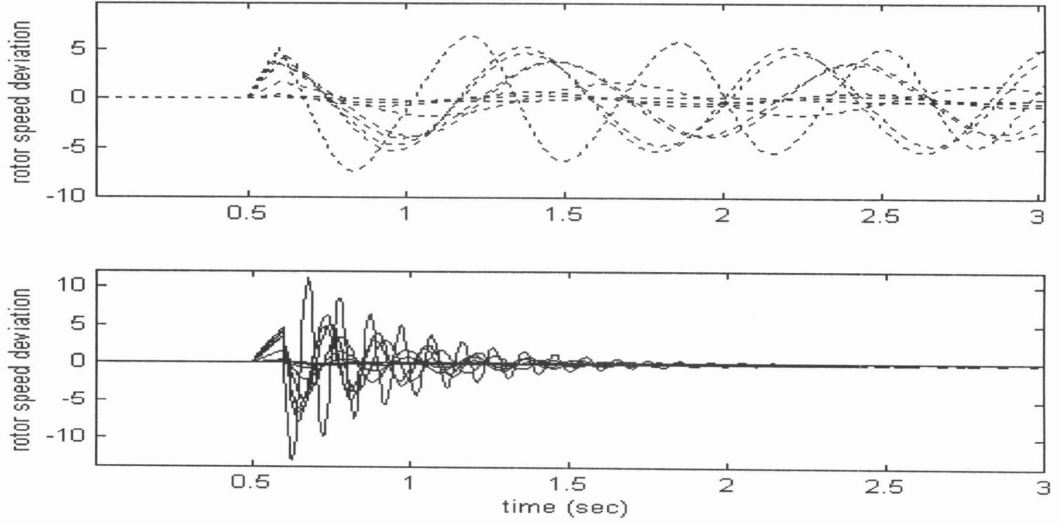


Figure 5.15: System responses to a three phase fault at the infinite bus applied for 100 ms ($T_{\Delta\omega_r/V_{ref}}$)

.... no controller — with PSS

The rotor speed deviation Figures 5.14 and 5.15 is given in radians per second.

5.5 Multi-machine PSS design

The distributed nature of large power systems makes the design of robust multi-machine power system stabilisers a formidable task. The problem is further constrained by measurements for each machine only being available locally for feedback. Interaction between the machines and controllers demand that the individual controller designs proceed in a co-ordinated manner. Various attempts have been made to circumvent the drawbacks associated with such a design task. The PSS design for multi-machine systems can be formulated as the decentralised stabilisation of a large-scale system problem. Yang, Zhang and Yu (1999) introduce the use of the structured singular value in a novel way to accomplish such decentralised designs. The structured singular value (SSV – ' μ ') is used to determine stability regions within which the closed loop system transfer function elements must lie to ensure that the designed controllers remain stabilising. The approach relies on results based on the SSV derived by Grosdidier and Morari (Yang *et al*, 1999). Rao and Boje (2001) have used a similar formulation to calculate these stability bounds in multi-machine PSS design to allow formulation within the QFT framework, and is the basis for the work contained in the example presented. More detail on the use of the SSV in stability boundary calculations in QFT is given in the course of this example.

The study system chosen to illustrate the design has previously been used by Klein *et al* (1991, 1992) to investigate the factors influencing the performance of power system stabilisers and to study the fundamental nature of inter-area oscillations. The next section provides an over-view of the four-machine study network. The effect of the inter-area mode, for a chosen operating point, on tie-line power flow is illustrated, highlighting the need for the application of PSS's.

5.5.1 The four machine study network

The system chosen to illustrate the design of PSS's for multi-machine networks is obtained from Kundur (1994, ch 12, p813), and has been shown to be insightful in system stability studies (Klein *et al*, 1991,1992) albeit of small size. This is a four-

machine network comprising of two areas connected by a dual circuit tie line. The machines in each area are identical. Figure 5.16 shows a line diagram of the network with the

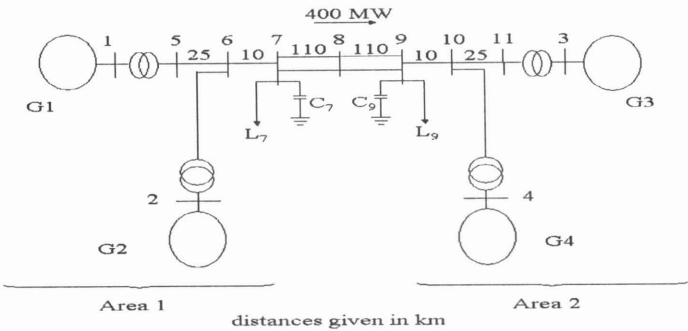


Figure 5.16: Two-area test case

machine data given in Appendix D.1. Four operating conditions are chosen for the design and are given in Table 5.1 (Rao and Boje, 2001). A generator outage scenario is included as one of the operating conditions. This case is chosen to illustrate how changes in the physical description of the network can be incorporated into the design with minimal effort. The nominal operating condition is chosen as Case A, in Table 5.1.

Case	Operating condition
A	Base case, area one exports 400MW to area two
B	Area one imports 400MW from area one
C	Base case with one of the parallel sections of 110km tie line out of circuit
D	Gen 4 o/c, load in area two reduced to 1130MW, area one exports 450MW to area two

Table 5.1: Operating conditions for the two-area system

For the nominal case, Area one exports 400 MW to Area two. The system possesses three oscillatory modes, two being local modes and the third being an inter-area mode. A non-linear implementation in PSCAD/EMTDC used throughout the study is shown in figure 5.17. The effect of the inter-area mode on the tie-line power flow for the nominal case is shown in figure 5.18. The first two seconds of the simulation is required by PSCAD/EMTDC for initialisation of the model. The inter-area mode

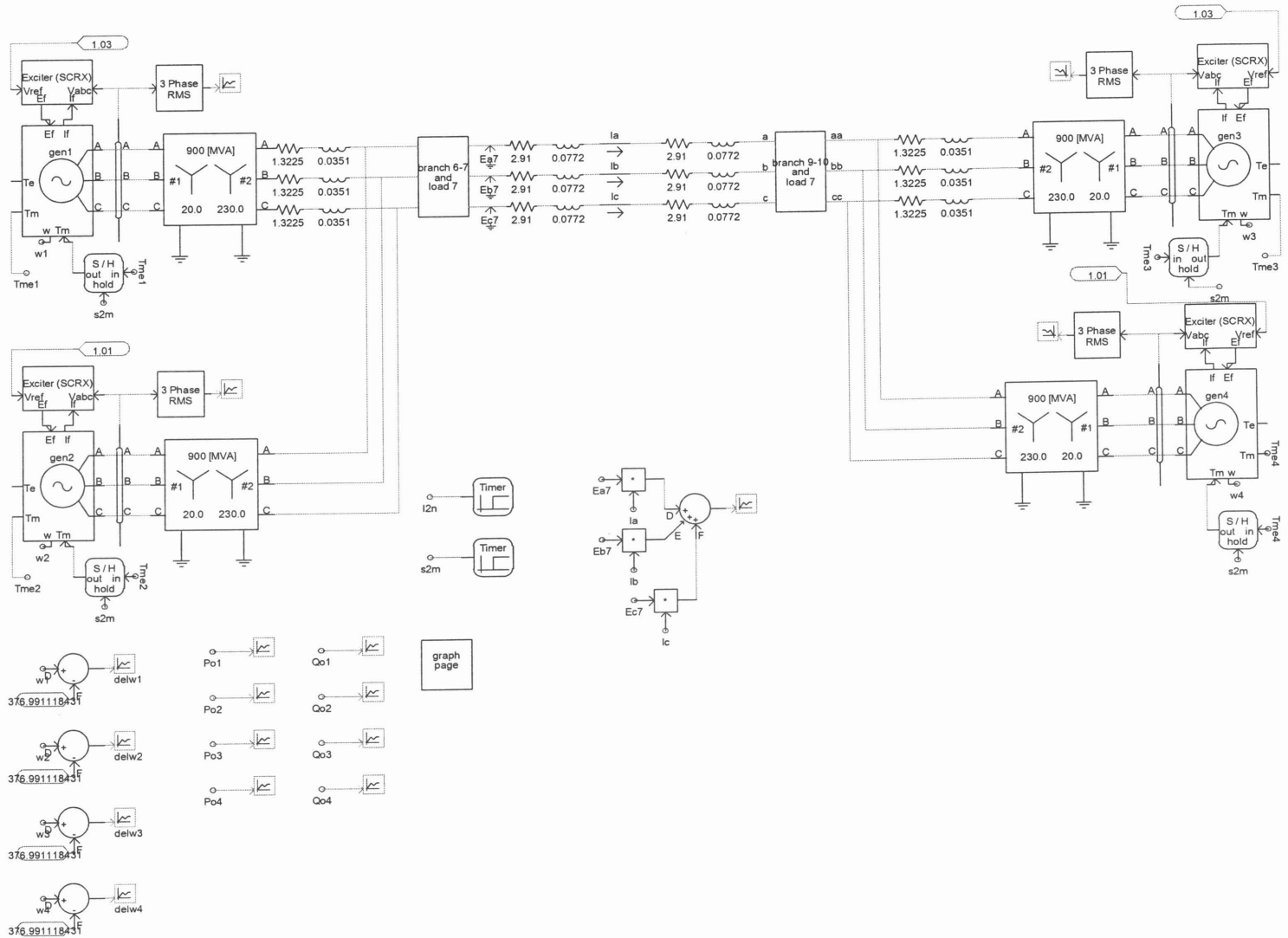


Figure 5.1.17: The PSCAD/EMTDC implementation of the two-area system

manifests itself as an oscillatory component of the tie line power. Chonco (2000) used a nonlinear formulation similar to that given in Figure 5.17 to investigate the use of FACTS devices to damp the inter-area mode oscillations in the same study network. In the design example, each generator is to be fitted with a PSS. To fit the design problem within the QFT framework, linearised models of the network are required to enable the formation of a template containing all possible plant descriptions. These can be

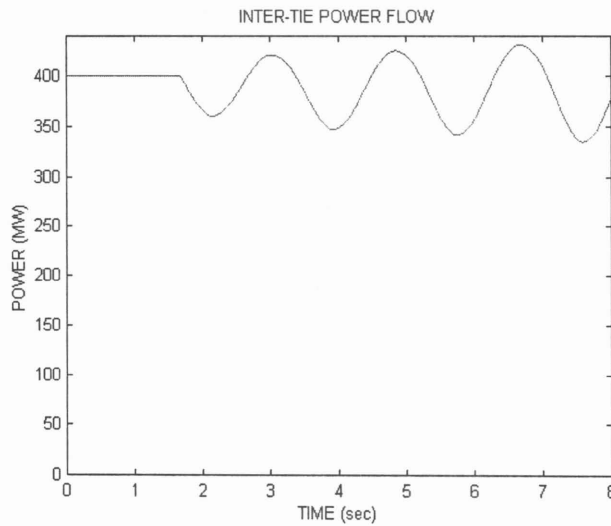


Figure 5.18: Effect of the inter-area mode on inter-tie power flow

obtained by using the 'Power System Toolbox' (Cherry Tree Scientific Software, 1993), with the bus and line data obtained from PSCAD/EMTDC. An illustration on obtaining the linearised model for Case A of Table 5.1 is shown in Appendix D.2. The linearised models for the design example were obtained from Rao (1998) due to the limited scope of this thesis.

5.5.2 The structured singular value as a stability measure

A MIMO plant represented by the $n \times n$ transfer function matrix $P(s)$, admitting a diagonal regular splitting, can be written as the sum of the diagonal and off-diagonal parts as follows:

$$\begin{aligned}\underline{P} &= \underline{P}_d + \underline{P}_o \\ &= (\underline{I} + \underline{P}_o \underline{P}_d^{-1}) \underline{P}_d\end{aligned}\quad 5.5.2.1$$

with the interaction matrix defined as

$$\underline{M} = \underline{P}_o \underline{P}_d^{-1} \quad 5.5.2.2$$

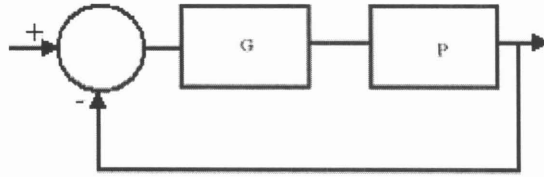


Fig 5.19: Equivalent feedback structure

If a diagonal stabilising controller, $\mathbf{G} = \text{diag}(g_{ii})_{i=1,2,\dots,n}$, exists as shown in figure 5.19, and the individual closed loop transfer functions can be defined as,

$$T = \text{diag}\left(\frac{p_{ii} g_{ii}}{1 + p_{ii} g_{ii}}\right) \quad 5.5.2.3$$

The closed loop system with the controller \mathbf{G} is stable under the following assumptions, (Yang *et al*, 1999; Rao *et al*, 2001),

- 1) The system does not have any unstable de-centralized fixed modes
- 2) \mathbf{P} and \mathbf{P}_d have an equal number of right half plane poles
- 3) The elements of \mathbf{T} are stable (by design)

if all elements of \mathbf{T} satisfy the following

$$|T_{ii}| < \frac{1}{\mu(\underline{M})} \quad \forall \quad i = 1, 2, \dots, n \quad 5.5.2.4$$

with $\mu(\bullet)$ being the SSV of the argument. This is a sufficient condition for stability of $T(s)$ provided the controller is designed based on the elements of P_d . This implies that each element, g_{ii} , must be designed independently on a single input-single output system P_{dii} . Equation 5.5.2.4 implies that for stability, the magnitude of the frequency response of the SISO closed loop elements of T must be less than a scalar frequency dependent function, $1/\mu(M(j\omega))$, (Yang *et al*, 1999). A toolbox is provided in MATLAB (Balas, Doyle, Glover and Packard, 1993) to calculate the SSV and has been used for all the calculations in the example presented. Equation 5.5.2.4 illustrates the use of the SSV to place magnitude bounds on the individual elements of T to ensure closed loop stability. The term on the right hand side of the inequality in equation 5.5.2.4 may be viewed as a circle within which all elements of T are constrained to lie to ensure stability.

5.6 Design example

All the participating generators in the test system affect the inter-area mode damping. The total damping will therefore be the sum of the contributions from the individual machines. As previously mentioned all generators are to be fitted with stabilisers in this example due to the small size of the study system. To incorporate the situation of a generator outage scenario requires minimal computational effort since the plant response is a complex number at every frequency. The design frequency range has been chosen to encompass the movement of the oscillatory modes with changing operating condition. The technique presented is a sequential design approach as each stabiliser is designed one a time. It should however be mentioned that this does not represent a sequential loop closure type approach.

The stability and performance bounds are calculated at each operating point and the intersection of these plotted on the Nichols chart is used as the design constraint.

5.6.1 Stability boundary calculations

The SSV has been shown in section 5.5.2 to be an effective way of computing stability bounds in design applications. Rao *et al* (2001), highlight that bounds computed in this manner can be rather conservative when applied to power systems that display high levels of inter-action between the diagonal and off-diagonal elements of the transfer function matrix. Applying equation 5.5.2.4 to the study system of figure 5.16 clearly highlights this shortcoming. This is demonstrated by figure 5.20 which shows the $\mu(M)$ for the example system of figure 5.16, plotted against the elements of T , for case A of Table 5.1. The shortcomings of using equation 5.5.2.4 to produce boundaries on the elements of T , are clearly evident around the inter-area mode frequency of 3.74 rad/sec. The bound is seen to be adequate at the higher local mode frequencies. The stabilising controller used is given by equation 5.5.6.2. The arguments presented are not entirely meaningless for application to power systems. Rao *et al* (2001) show that instead of placing a bound on the diagonal elements of the closed loop transfer function, it is possible to use a similar formulation to generate the required bounds on the controller frequency response.

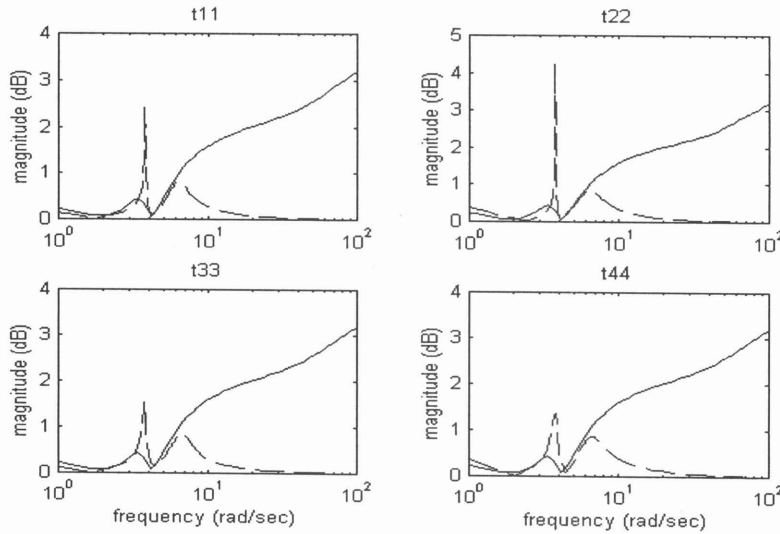


Figure 5.20: ---- Magnitude of the elements of T , '—' $1/\mu(M)$

This may be accomplished in the following manner. If a nominal controller G_o exists, such that application to the individual input/output pairs in P results in stable

closed loops, and $\Delta = \text{diag}(\Delta_{ii})$ is an additive perturbation in the controller matrix, shown in figure 5.21,

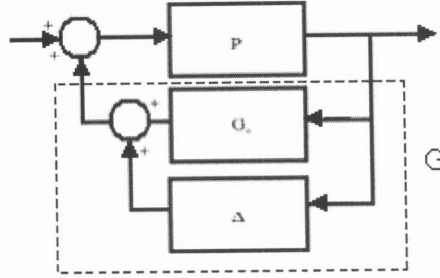


Figure 5.21: Nominal PSS with added perturbation

Using the definition of the structured singular value (Rao *et al*, 2001) the system remains stable if,

$$|\Delta_{ii}| < \frac{1}{\mu(\underline{P}(\underline{I} - \underline{G}_o \underline{P})^{-1})} \quad 5.5.6.1$$

This once again generates circular regions, now centred at g_{oi} , at every frequency. The radius is given by the term on the right of the in-equality. The intersection over the plant set of these circles at each frequency is the region within which all stabiliser responses must lie to ensure stability of the closed loop system. The stabilising controller for this study network is obtained from Klein *et al* (1992) and is given by,

$$g_{oi} = 20 \frac{10s}{1+10s} \frac{1+0.05s}{1+0.02s} \frac{1+3s}{1+5.4s} \quad 5.5.6.2$$

Applying equation 5.5.6.1 to the example system, the stability bound on PSS design at the inter-area mode frequency of 3.74 rad/sec is shown in figure 5.22. In the chosen example the stabilising controller is identical for all machines. The controller is thus given by $\underline{G}_o = g_{oi}\underline{I}$, where the identity matrix is of the same dimension as \underline{P} . For multiple operating conditions the bound for robust stability is

the intersection of the bounds calculated at each operating condition. In the example system, since the stabilising controller is identical for all machines, all the circles are centred at the same point, g_{oi} , and the stability bound becomes the circle of minimum radius.

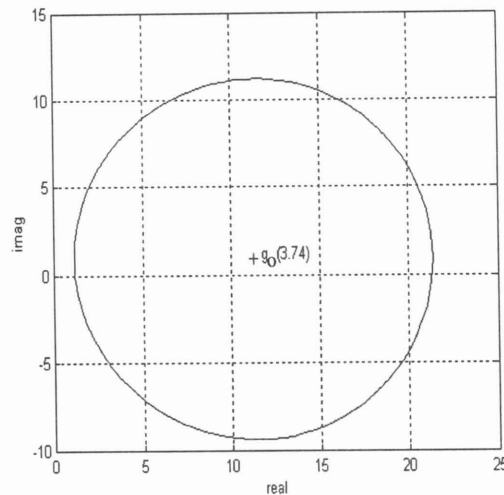


Figure 5.22: Stability bound on PSS response
at the inter-area mode frequency

5.6.2 Determining the performance specifications

The application of PSS's is not only necessitated by the requirement for system stability. An improvement in the closed loop performance is also generally desired. In this design example the requirement is for a stabilising PSS that enhances the overall system damping, thereby improving the closed loop performance. The open loop transfer functions from the AVR to rotor speed for each individual machine demonstrates behaviour that contains magnitude peaks at the modal frequencies. This is due to inadequate damping of the dominant poles. Specifications on the closed loop performance may be generated in any number of realistic ways for use within the QFT framework. The specifications in this illustrative example are formulated along the lines presented in Rao *et al* (2001). Since the design of each stabiliser is treated as a SISO design, it is possible to impose performance

restrictions only on the diagonal elements of the transfer function matrix to achieve the desired effect. Placing upper bounds on the closed loop magnitude of the diagonal elements, at the modal frequencies will increase the damping and give the required performance improvement. In the design example the off diagonal elements contain the same dominant poles as the diagonal elements of the transfer function matrix. Therefore, an improvement in the damping of the diagonal elements will guarantee improvement in the damping of the off diagonal elements. The chosen specifications on the closed loop magnitudes can be converted into bounds on the controller frequency response, (Rao *et al*, 2001). For example, a SISO plant with open loop transfer function $p(s)$, and a controller $g(s)$ with positive feedback has the closed loop transfer function given by,

$$t(j\omega) = p(j\omega)(1 - p(j\omega)g(j\omega))^{-1} \quad 5.6.2.1$$

If the magnitude of $t(j\omega)$ is to be bounded by a function $a(\omega)$, equation 5.6.2.1 can be written as

$$|t(j\omega)| = |p(j\omega)(1 - p(j\omega)g(j\omega))^{-1}| < a(\omega) \quad \forall \omega$$

or

$$|t^{-1}(j\omega)| = |p^{-1}(j\omega) - g(j\omega)| > a^{-1}(\omega) \quad \forall \omega \quad 5.6.2.2$$

Equation 5.6.2.2 defines a circular region of radius $a^{-1}(\omega)$ centred at the point $p^{-1}(j\omega)$ outside of which the controller response, $g(j\omega)$, should lie. These regions are easily transferred onto the Nichols chart, using *genbnds*(10,...), for use in a normal QFT type design. If the intention is to only directly affect the dominant pole damping, the performance bounds may be obtained by simply replacing the dominant poles in the plant, $p(s)$, with poles of the same frequency and the desired damping factor (Rao *et al*, 2001). The magnitude plot of the transfer function for generator one's AVR input to speed output for Case A of Table 5.1, is shown in

figure 5.23, compared with the same function when the dominant poles are replaced with poles of the same frequency and damping factor of 5%.

It is important to bear in mind that bounds calculated in this manner are operating point dependent. At each operating point, the useful boundary is the intersection of the individual bounds.

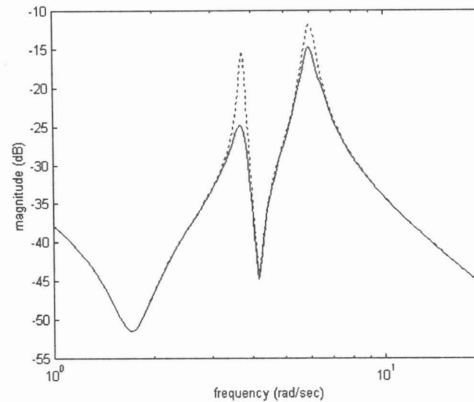
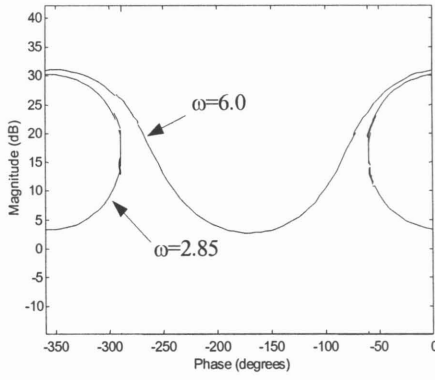
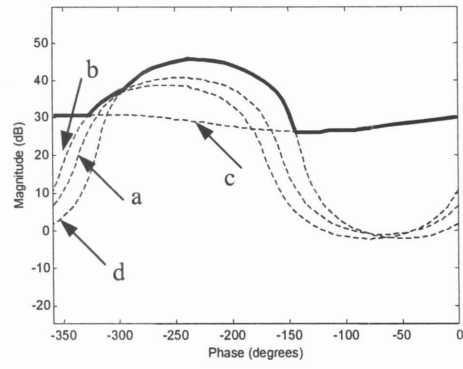


Figure 5.23: ···· Magnitude plot of the plant element
— Plot of the modified function

An example of the stability and performance bounds on the Nichols chart, for Case A, is shown in figure 5.24. The controllers are designed to lie in the intersection of the stability and performance bounds at each frequency. Figure 5.25(a) illustrates the intersection of the boundary regions for Case A, plotted at $\omega = 2.85$ rad/sec. The regions of intersection between the stability and performance bounds may be very small or even not possible. The gain of the nominal controller can be increased resulting in an upward shift of the stability bounds on the Nichols chart. The only condition is that the nominal controller still stabilises the plant. The performance requirements can also be adjusted for more realistic damping of each system mode. The overall damping for the inter-area mode should however not become too small as this negates the entire design objective. The plot of the designed controller for generator one is shown in figure 5.25(b) together with the specifications for Case A.



(a)



(b)

Figure 5.24: (a) - Stability bounds

(b) Performance bounds at 2.85 rad/sec
— Intersection of performance bounds
for case (a)-(d)

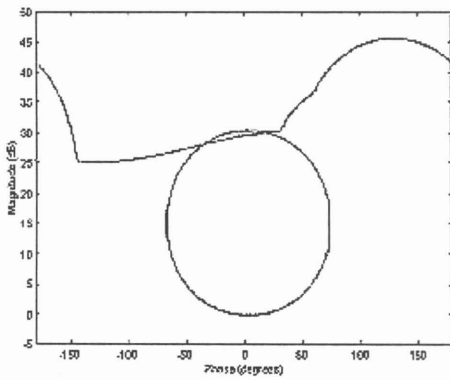
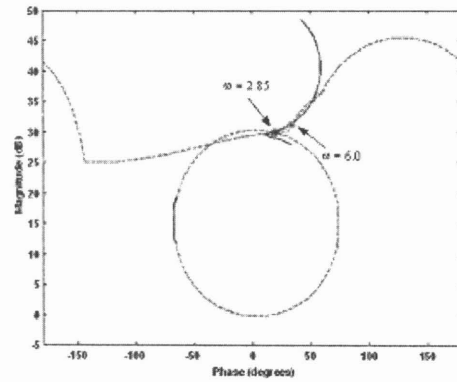


Figure 5.25: (a) intersection of design
boundaries



(b) ---- design boundaries
— designed controller

The equation of the final diagonal controller meeting all the specifications has the elements given below:

$$g_{ii} = 30 \frac{10s}{(10s+1)} \frac{0.1211s+1}{(0.00925s+1)} \quad i = 1,2$$

$$g_{ii} = 12.5 \frac{10s}{(10s+1)} \frac{0.1523s+1}{(0.0073s+1)} \quad i = 3,4$$

The controller performance for small disturbances at the AVR reference input of each generator for all the operating conditions is shown in figure 5.26. The network is then subjected to a large disturbance in the form of a three phase to ground fault at bus eight. The system response to the large disturbance for all operating conditions is shown in figure 5.27.

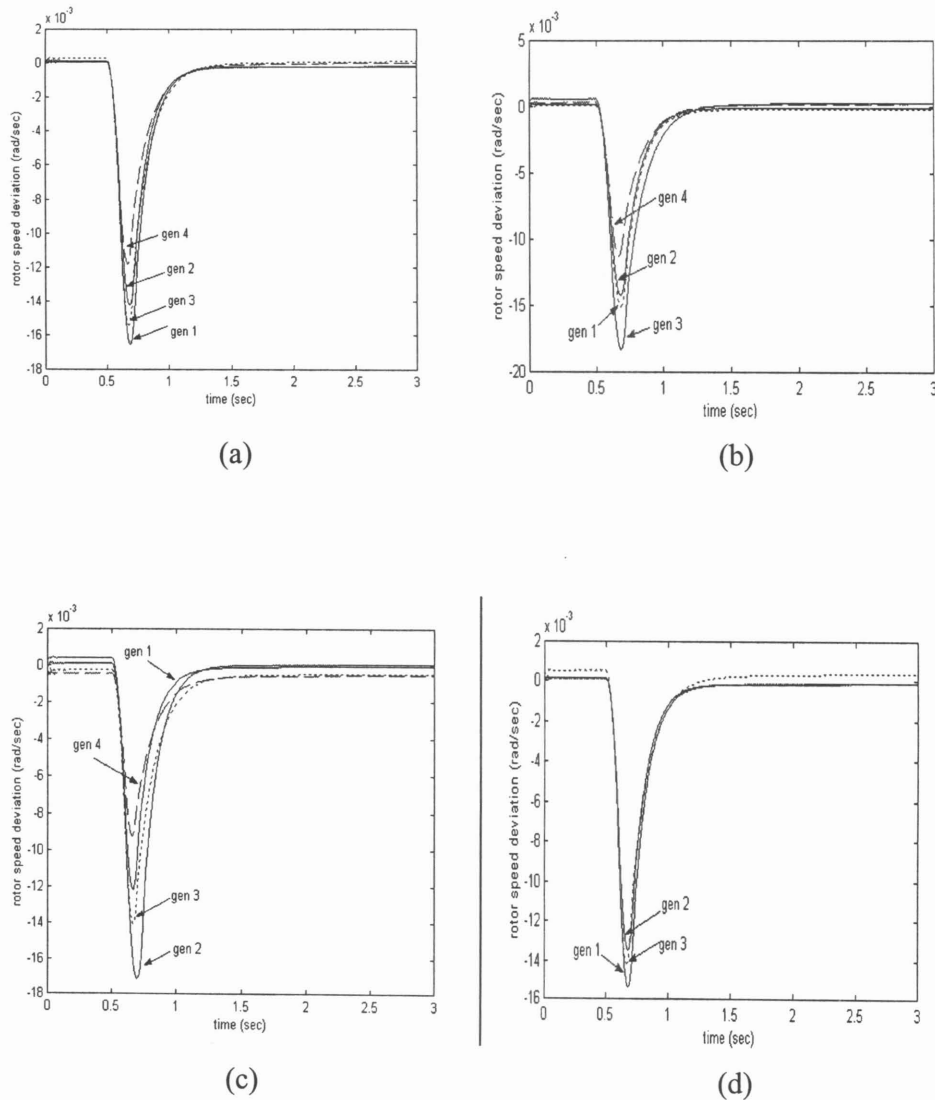


Figure 5.26: System responses to a 5% step disturbance at the AVR input of all generators for 100 ms : cases a-d

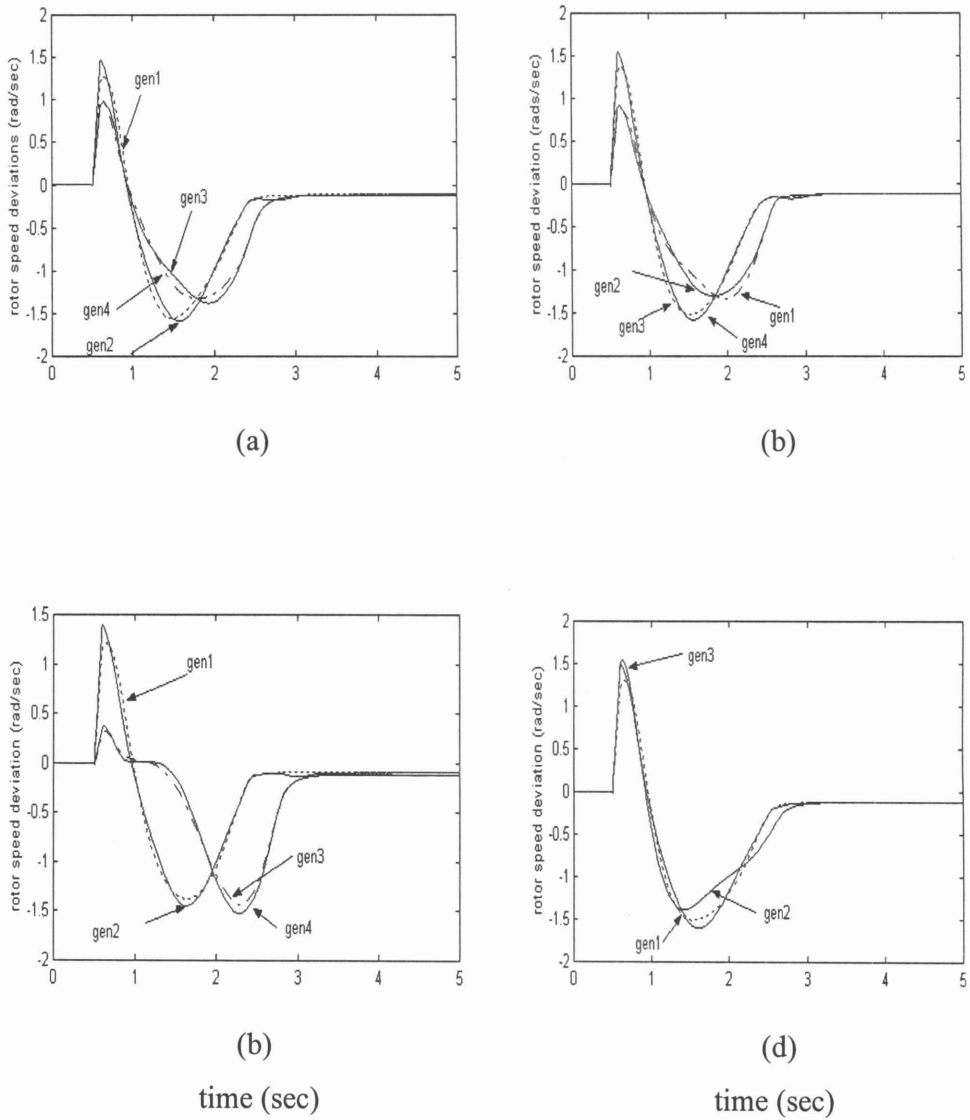


Figure 5.27: System responses to a three phase fault at bus no 8 applied for 100 ms. cases a-d

5.7 Conclusion

This chapter has shown the use of QFT for robust damping controller design. The development from the single-input single-output to the multivariable case is illustrated. The problem of damping controller design for multi-machine power systems has been examined using a four-machine study system (Klein *et al*, 1992; Kundur, 1994). The necessary extensions required to enable multi-machine damping controller design within the QFT framework is introduced (Rao *et al*, 2001) and used to accomplish PSS design for the study network.

The time-domain simulations are undertaken with a detailed model in PSCAD/EMTDC. These simulations were used to assess the controller performance at each of the chosen operating conditions. The results show that the designed controller meets the requirements of being both stabilising and enhancing the closed loop performance.

The effect of different load models has not been investigated. The outlined methodology can be easily extended to incorporate different load models. As the load model changes the corresponding linearised system description will change to reflect this. These are then added to the description of the system uncertainty in the manner outlined in this chapter.

In multi-machine power networks damping controllers may not be required on every machine. Damping controllers need only be applied to machines participating in a specific oscillatory mode. The identification of these of these generators commonly relies on residue techniques and participation factors. This topic has not been investigated since all generators participate in the unstable inter-area mode of this example. The poorly damped local modes are also well damped after the addition of the stabilisers.

The next chapter makes concluding remarks on the thesis in its entirety and outlines the scope for further work.

CHAPTER SIX

Conclusion

This thesis has illustrated the design of power system damping controllers using three different approaches. This chapter discusses their relative merits, and concludes with some suggestions for further work.

6.1 Comparative analysis

Chapter Three illustrated the conventional PSS design methodology applied to the design of a damping controller for a SMIB system over a restricted range of operating conditions. The ease of application of the conventional design method is overshadowed by its lack of robustness considerations during the design process. For controllers designed in this manner the design operating point must be very carefully chosen. This may prevent the controller exciting other potential oscillatory modes that exist elsewhere in the frequency domain due to the changing operating conditions.

Chapter Four introduced the first of two robust design methods for robust PSS design. H_∞ optimisation has been shown to be effective in producing a robust controller for a restricted range of operating conditions. One shortfall of this method is that it can be very conservative for robust stability analysis and cannot explicitly handle pole-placement type specifications. The choice of the weighting functions for minimisation of the system norms is also of paramount importance during the design process. The order of the controllers generated are dependent on the order of the plant model and weighting function used and is generally of unnecessarily high order. The order of the synthesized controller increases with an increase in order of the plant and weighting function description. This may make the controllers practically unrealisable when high order plant and load models are required. The excitation system used in the plant

description during the design was a high gain static model. In practice there may for example be necessary requirements for the addition of transient gain reduction, which results in a corresponding increase in controller order. Care needs to be taken to define the plant uncertainty in a meaningful way without violating the standard definition within the H_∞ formulation. If the operating range increases, the uncertainty description increases and a new weighting function is required to adequately describe the deviation from a nominal plant model. This makes dealing with added operating conditions labour intensive once the design process has begun.

QFT is shown in Chapter Five to be effective in the design of stabilizers for the SMIB and the multi-machine cases. In the design of the PSS for the SMIB case, the design proceeds with ease once the specifications in the frequency domain are adequately defined. The model uncertainty has an accurate description as opposed to that of H_∞ outlined above. Increases in plant and load model order are also easily dealt with, as the plant description is a simply complex number at every frequency. PSS design was also outlined for a multi-machine study network displaying both local and inter-area modes. The decentralized nature of the design problem in the multi-machine case makes it difficult to find meaningful stability boundaries for the design. The structured singular value has been shown to be useful in alleviating such drawbacks. A stabilizing controller has been successfully designed for the four-machine test system. A PSCAD/EMTDC implementation was devised and used for the performance assessment of the designed controller.

6.2 Suggestions for further work

The thesis has shown two approaches to robust controller design. The limited scope of the thesis made it impossible to deal with all aspects and was confined to the key considerations contained herein. In a full research thesis it may be appropriate to conduct laboratory testing of all the designed controllers. The development of linearised models for the four-machine test system was also beyond the scope of this thesis and

more accurate models can be found. This will ensure that the designed controllers reflect more accurately controllers that may be implemented in practice. The design specifications together with practical operating ranges may also be obtained from a reputable power utility to facilitate a realistic design that will result in practical laboratory simulations.

Appendix A

Modelling of the SMIB system

The following model of a single machine infinite bus (SMIB) system is obtained from Kundur (1994) and is included for ease of reference. The meaning of symbols can be found in the list of symbols at the beginning of the thesis. All quantities are in per unit unless otherwise stated.

The general configuration for a single generator connected to an infinite bus via a transmission line, with line resistance ignored, is shown below

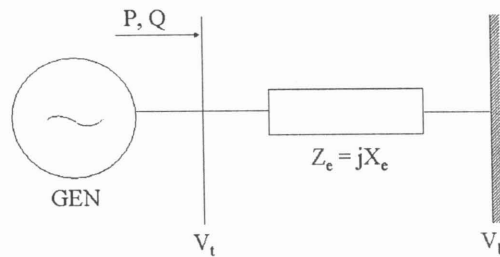


Figure A.1: schematic of the SMIB system

The damper winding and stator transient effects are ignored in the following discussion but can be added easily in the frequency domain design.

The generator in figure A.1, without an automatic voltage regulator and excitation system can be described by the equations given below. The numbers within brackets represent the numbering in the reference (Kundur, 1994).

$$\Delta \dot{\omega}_r = \frac{1}{2H} (\Delta Tm - K_1 \Delta \delta - K_D \Delta \omega_r - K_2 \Delta \psi_{fd}) \quad \text{A.1.1 (12.115)}$$

$$\Delta \dot{\delta} = \omega_o \Delta \omega_r \quad \text{A.1.2 (12.115)}$$

$$\Delta \dot{\psi}_{fd} = -\frac{\omega_o R_{fd}}{L_{fd}} m_1 L'_{ads} \Delta \delta - \frac{\omega_o R_{fd}}{L_{fd}} \left[1 - \frac{L'_{ads}}{L_{fd}} + m_2 L'_{ads} \right] \Delta \psi_{fd} \quad \text{A.1.3 (12.115)}$$

where

$$m_1 = \frac{E_B (X_{Tq} \sin \delta_0 - R_T \cos \delta_0)}{R_T^2 + X_{Tq} X_{Td}} \quad \text{A.1.4 (12.108)}$$

and

$$m_2 = \frac{X_{Tq}}{R_T^2 + X_{Tq} X_{Td}} \frac{L_{ads}}{(L_{ads} + L_{fd})} \quad \text{A.1.5 (12.108)}$$

$$n_1 = \frac{E_B (R_T \sin \delta_0 + X_{Td} \cos \delta_0)}{R_T^2 + X_{Tq} X_{Td}} \quad \text{A.1.6 (12.108)}$$

$$n_2 = \frac{R_T}{R_T^2 + X_{Tq} X_{Td}} \frac{L_{ads}}{(L_{ads} + L_{fd})} \quad \text{A.1.7 (12.108)}$$

The effect when field excitation control with a AVR added, is illustrated in the block diagram below (Kundur, 1994; p 759)

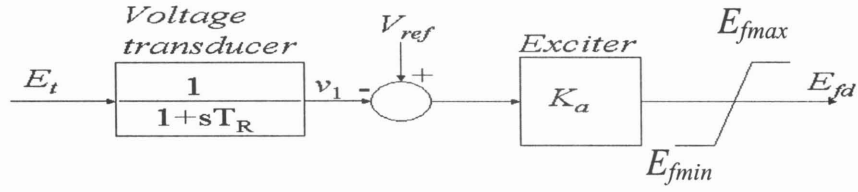


Figure A.2: Thyristor excitation system with AVR

The terms E_{fmax} and E_{fmin} in figure A.2 above is added to exciters implemented practically to prevent saturation of the field in any direction. Field saturation effects were not considered during the course of this thesis. The differential equation describing the state variable associated with the AVR is

$$\dot{\Delta v_1} = \frac{K_5}{T_R} \Delta \delta + \frac{K_6}{T_R} \Delta \psi_{fd} - \frac{1}{T_R} \Delta v_1 \quad \text{A.1.8 (12.135)}$$

Taking into account the effect of the exciter and the AVR on equations A.1.1-A.1.3, the complete state-space description, with ΔT_m equal to zero, is given by

$$\begin{bmatrix} \dot{\Delta \omega_r} \\ \dot{\Delta \delta} \\ \dot{\Delta \psi_{fd}} \\ \dot{\Delta v_1} \end{bmatrix} = \begin{bmatrix} -\frac{K_D}{2H} & -\frac{K_1}{2H} & -\frac{K_2}{2H} & 0 \\ \omega_0 & 0 & 0 & 0 \\ 0 & -\frac{K_3 K_4}{T_3} & -\frac{1}{T_3} & -\frac{K_3 K_a}{T_3} \\ 0 & \frac{K_5}{T_R} & \frac{K_6}{T_R} & -\frac{1}{T_R} \end{bmatrix} \begin{bmatrix} \Delta \omega_r \\ \Delta \delta \\ \Delta \psi_{fd} \\ \Delta v_1 \end{bmatrix} + \begin{bmatrix} 0 \\ 0 \\ \frac{K_3 K_a}{T_3} \\ 0 \end{bmatrix} V_{ref} \quad \text{A.1.9 (a)}$$

With the rotor speed deviation chosen as the output of interest

$$C = [1 \ 0 \ 0 \ 0], \quad D = [0] \quad \text{A.1.9 (b)}$$

The formulae for the constants K_1 - K_6 are given below

$$K_1 = \frac{E_B E_{q0}}{R_T^2 + X_{Tq} X_{Td}} (R_T \sin \delta_0 + X_{Td} \cos \delta_0) + \frac{E_B i_{q0}}{R_T^2 + X_{Tq} X_{Td}} (X_{Tq} \sin \delta_0 - R_T \cos \delta_0) \quad (12.123)$$

$$K_2 = \frac{L_{ads}}{L_{ads} + L_{fd}} \left[\frac{R_T}{R_T^2 + X_{Tq} X_{Td}} E_{q0} + \left(\frac{X_{Tq} (X_q - X'_d)}{R_T^2 + X_{Tq} X_{Td}} + 1 \right) i_{q0} \right] \quad (12.124)$$

$$K_3 = \frac{L_{ads} + L_{fd}}{L_{adu}} \left(1 + \frac{X_{Tq}}{R_T^2 + X_{Tq} X_{Td}} (X_d - X'_d) \right)^{-1} \quad (12.126)$$

$$T_3 = T_{d0s} \left(1 + \frac{X_{Tq}}{R_T^2 + X_{Tq} X_{Td}} (X_d - X'_d) \right)^{-1} \quad (12.127)$$

$$K_4 = L_{adu} \frac{L_{ads}}{L_{ads} + L_{fd}} \frac{E_B}{R_T^2 + X_{Tq} X_{Td}} (X_{Tq} \sin \delta_0 - R_T \cos \delta_0) \quad (12.128)$$

$$K_5 = \frac{e_{d0}}{E_{t0}} [-R_a m_1 + L_l n_1 + L_{aqs} n_1] + \frac{e_{q0}}{E_{t0}} [-R_a n_1 - L_l m_1 - L'_{ads} m_1] \quad (12.133)$$

$$K_6 = \frac{e_{d0}}{E_{t0}} [-R_a m_2 + L_l n_2 + L_{aqs} n_2] + \frac{e_{q0}}{E_{t0}} [-R_a n_2 - L_l m_2 - L'_{ads} (\frac{1}{L_{fd}} - m_2)] \quad (12.134)$$

where

$$R_T = R_a + R_e \quad (12.105)$$

$$X_{Tq} = X_e + (L_{aqs} + L_l) \quad (12.105)$$

$$X_{Td} = X_e + (L'_{ads} + L_l) \quad (12.105)$$

and the subscript 's' denotes the saturated value of a quantity. All quantities are given in per unit. The block diagram representation of the SMIB system is shown below

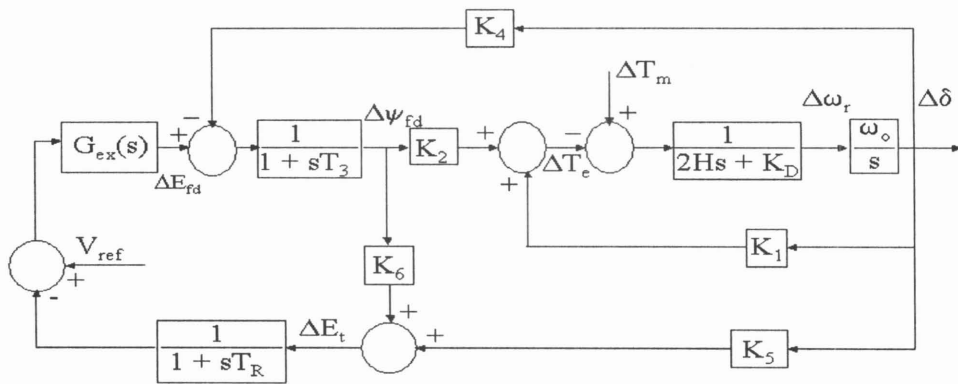


Figure A.3: SMIB block diagram

Appendix B

B.1 : System data

This appendix gives the parameters for the single machine infinite bus system (Kundur, 1994; p 732,752) used in the examples presented in this thesis. All quantities are in per unit unless otherwise stated.

Generator

$$R_a = 0.003$$

$$X_d = 1.81$$

$$X_q = 1.76$$

$$X_l = 0.16$$

$$X'_d = 0.3$$

$$T'_{d0} = 8.0 \text{ sec}$$

$$H = 3.5$$

$$K_D = 0$$

$$\omega_0 = 377 \text{ rad / sec}$$

$$V_b = 1.0$$

AVR and exciter

$$K_a = 200$$

$$T_R = 0.01 \text{ sec}$$

Base power = 2220 MVA

Base voltage = 24 kV

B.2 : K constants

This appendix gives the 'K' constants for the example of Chapter Three. These are operating point and system dependent and correspond to the operating point and system parameters used in the example of Chapter Three.

$$K_1 = 1.23$$

$$K_2 = 0.874$$

$$K_3 = 0.26$$

$$K_4 = 2.58$$

$$K_5 = -0.015$$

$$K_6 = 0.23$$

$$K_a = 200$$

$$T_3 = 2.0$$

$$T_R = 0.01\text{sec}$$

B.3: System description for the extended range of operating conditions

This appendix gives the transfer function matrix description as used in the design of section 5.2. The machine is described by a third order model (Kundur, 1994) and the equations are obtained from Boje *et al* (1999). The governor and AVR description used to close the speed and voltage loops before the design of the PSS can commence is also given.

$$\begin{pmatrix} \Delta\omega(s) \\ \Delta V_t(s) \end{pmatrix} = P(s) \begin{pmatrix} \Delta T_m(s) \\ \Delta E_{fd}(s) \end{pmatrix}$$

$$P(s) = \frac{1}{\Delta(s)} \begin{pmatrix} \tilde{p}_{11} & \tilde{p}_{12} \\ \tilde{p}_{21} & \tilde{p}_{22} \end{pmatrix}$$

with

$$\begin{aligned}\tilde{p}_{11}(s) &= (1 + sK_3T'_{d0})s \\ \tilde{p}_{12}(s) &= -K_2K_3s \\ \tilde{p}_{21}(s) &= K_5(1 + sK_3T'_{d0})\omega_0 - K_2K_4K_6\omega_0 \\ \tilde{p}_{22}(s) &= K_3[K_6(Ms + K_D)s + (K_1K_6 - K_2K_5)\omega_0]\end{aligned}$$

and

$$\Delta(s) = (Ms + K_D)(1 + sK_3T'_{d0})s + K_1(1 + sK_3T'_{d0})\omega_0 - K_2K_3K_4\omega_0$$

$$M = 2H$$

The AVR and governor are given as follows,

$$G_1 = \begin{pmatrix} g_G & 0 \\ 0 & g_E \end{pmatrix}$$

where

$$g_G = \frac{k_g}{s(sT_g + 1)(sT_t + 1)}$$

$$g_E = \frac{k_a}{(sT_R + 1)}$$

The governor constants are as follows,

$$k_g = 1, \quad T_g = 0.22s, \quad T_t = 0.30s$$

The constants for the AVR are as given in Appendix B.2.

Appendix C

Glover-Doyle solution to the standard H_∞ problem

The solution to the problem statement of chapter 4 is outlined here. This solution is taken from Rao (1998, p 119-121)

Consider the generalized plant shown in the figure below

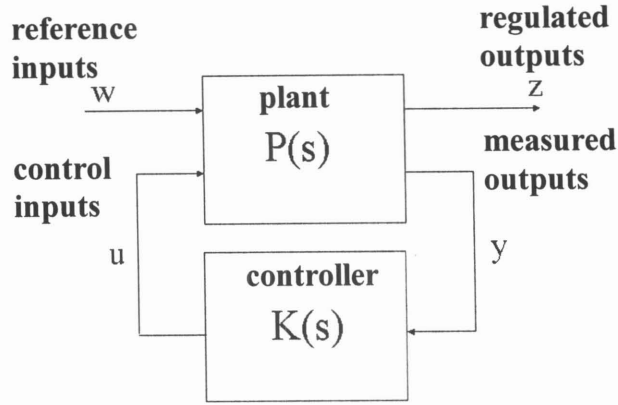


Figure C.1: generalized plant model

Let the plant P have the following realization

$$\dot{x} = Ax + B_1 w + B_2 u$$

$$z = C_1 x + D_{11} w + D_{12} u$$

$$y = C_2 x + D_{21} w + D_{22} u$$

The set of equations above can be represented as follows

$$P = \begin{bmatrix} A & B_1 & B_2 \\ \hline C_1 & D_{11} & D_{12} \\ C_2 & D_{21} & D_{22} \end{bmatrix}$$

The following assumptions are made,

1. (A, B_2) is stabilizable and (A, C_2) is detectable
2. $D_{11} = 0, D_{22} = 0$
3. $D_{12} = \begin{bmatrix} 0 \\ I \end{bmatrix}, D_{21} = \begin{bmatrix} 0 & I \end{bmatrix}$
4. $D_{12}^T C_1 = 0, B_1 D_{21}^T = 0$

Assumptions 2 and 4 can be relaxed except for the requirement that the matrices, D_{12} , and D_{21} have full column and row ranks respectively.

Under these assumptions, given a value $\gamma > 0$, there exists a stabilizing controller K such that $\|T_{wz}\|_\infty < \gamma$ if and only if

- a. There exists a symmetric and positive semi-definite solution, $X_\infty = X_\infty^T \geq 0$, satisfying

$$X_\infty A + A^T X_\infty - X_\infty (\gamma^{-2} B_1 B_1^T - B_2 B_2^T) X_\infty + C_1^T C_1 = 0 \quad \text{C.1.1}$$

with $(A + (\gamma^{-2} B_1 B_1^T - B_2 B_2^T) X_\infty)$ stable,

- b. There exists a symmetric and positive semi-definite solution, $Y_\infty = Y_\infty^T \geq 0$, satisfying

$$Y_\infty A^T + AY_\infty - Y_\infty (\gamma^{-2} C_1^T C_1 - C_2^T C_2) Y_\infty + B_1 B_1^T = 0 \quad \text{C.1.2}$$

with $(A^T + (\gamma^{-2} C_1^T C_1 - C_2^T C_2) Y_\infty)$ stable,

- c. $\rho(X_\infty Y_\infty) < \gamma^2$, where $\rho(\bullet)$ represents the spectral radius of the argument.

There exist standard techniques to solve the algebraic Ricatti equations C.1.1 and C.1.2.

If the above conditions hold, a solution is the controller with the realization

$$K = \begin{bmatrix} \hat{A}_\infty & -Z_\infty L_\infty \\ F_\infty & 0 \end{bmatrix} \quad \text{C.1.3}$$

where

$$\hat{A}_\infty = A - \gamma^{-2} B_1 B_1^T X_\infty + B_2 F_\infty + Z_\infty L_\infty C_2$$

$$F_\infty = -B_2^T X_\infty$$

$$L_\infty = -Y_\infty C_2^T$$

$$Z_\infty = (I - \gamma^{-2} Y_\infty X_\infty)^{-1}$$

This is the central or minimum entropy controller and has been used in the solution to the problem presented in this thesis.

For H_∞ norm minimization, the conditions a-c are solved repeatedly with varying values of γ , until the optimum value is approached to within the desired level of tolerance. The controller is then a realization of the corresponding solutions, X_∞ and Y_∞ .

Appendix D

D.1 : Parameters of the two area system

This appendix gives the parameters for the two-area system in Chapter Five (Kundur, 1994; p 813). All quantities are in per unit unless otherwise stated.

Generator

$$\begin{aligned}
 X_d &= 1.8 & X_q &= 1.7 & X_l &= 0.2 & X'_d &= 0.3 & X'_q &= 0.55 \\
 X''_d &= 0.25 & X''_q &= 0.25 & R_a &= 0.0025 & T'_{d0} &= 8.0 \text{ sec} & T'_{q0} &= 0.4 \text{ sec} \\
 T''_{d0} &= 0.03 \text{ sec} & T''_{q0} &= 0.05 \text{ sec} & A_{sat} &= 0.015 & B_{sat} &= 9.6 & \psi_{T1} &= 0.9 \\
 H &= 6.5 \text{ (for G1 and G2)} & H &= 6.175 \text{ (for G3 and G4)} & K_D &= 0 \\
 \text{Base power} &= 900 \text{ MVA} & \text{Base voltage} &= 20 \text{ kV}
 \end{aligned}$$

Transmission line

The line lengths are given in figure 5.16

$$r = 0.0001 \text{ pu/km} \quad x_L = 0.001 \text{ pu/km} \quad b_C = 0.00175 \text{ pu/km}$$

$$\text{Base power} = 100 \text{ MVA} \quad \text{Base voltage} = 230 \text{ kV}$$

Transformers

$$R_T = 0.0 \quad X_T = 0.15$$

$$\text{Base power} = 900 \text{ MVA} \quad \text{Base voltage} = 20/230 \text{ kV}$$

The following data is given for Case a of table 5.3

Initial conditions of the generators

G1: $P = 700$ MW	$Q = 185$ MVA	$E_t = 1.03 \angle 20.2^\circ$
G2: $P = 700$ MW	$Q = 235$ MVA	$E_t = 1.01 \angle 10.5^\circ$
G3: $P = 719$ MW	$Q = 176$ MVA	$E_t = 1.03 \angle -6.8^\circ$
G4: $P = 700$ MW	$Q = 202$ MVA	$E_t = 1.03 \angle -17.0^\circ$

System loads

Bus 7: $P_L = 967$ MW	$Q_L = 100$ MVA	$Q_C = 200$ MVA
Bus 9: $P_L = 1767$ MW	$Q_L = 100$ MVA	$Q_C = 350$ MVA

Thyristor exciter with transient gain reduction (TGR)

- $K_A = 200$
- $T_A = 1.0$ sec
- $T_B = 10.0$ sec
- $T_R = 0.01$ sec

D.2: The Power System Toolbox

The following is an illustration on using the Power System Toolbox to generate linearized models of the system shown in figure 5.16. The data set presented here has been generated for Case A of Table 5.1 using PSCAD/EMTDC. The base power is chosen as 100 MVA.

For a more in depth discussion on advanced features the relevant user manual should be consulted.

```
%*****
%data from PSCAD for use with the power system toolbox to generate
%linearised models
%the sub-transient machine model is used.
%the exciter is a thyristor type with transient gain reduction

bus = [1 1.03    20.2    7.0    1.85 0      0 0 0 2  5.0  -2.0  20;
       2 1.01    10.5    7.0    2.35 0      0 0 0 2  5.0  -2.0  20;
       3 1.03    -6.8    7.19 1.76 0      0 0 0 1  5.0  -2.0  20;
       4 1.01   -17     7.0    2.02 0      0 0 0 2  5.0  -2.0  20;
       5 1.0023  13.93 0      0      0      0 0 0 3  0.0   0.0  230;
       6 0.9737  4.14 0      0      0      0 0 0 3  0.0   0.0  230;
       7 0.9549 -3.83 0      2.0  9.67 1  0 0 3  4.0   0.0  230;
       8 0.9342 -17.95 0      0.0  0      0 0 0 3  0.0   0.0  230;
       9 0.9730 -30.86 0      3.5  17.67 1  0 0 3  4.0   0.0  230;
      10 0.9854 -23.08 0      0      0.00 0  0 0 3  0.0   0.0  230;
      11 1.0063 -13.19 0      0      0.00 0  0 0 3  0.0   0.0  230];

line = [...
1   5   0.0      0.0167   0.00      0 0 0 0 0;
5   6   0.0025   0.025    0.00      0 0 0 0 0;
2   6   0.0      0.0167   0.00      0 0 0 0 0;
6   7   0.001    0.01     0.00      0 0 0 0 0;
7   8   0.011    0.110    0.00      0 0 0 0 0;
7   8   0.011    0.110    0.00      0 0 0 0 0;
9   8   0.011    0.110    0.00      0 0 0 0 0;
9   8   0.011    0.110    0.00      0 0 0 0 0;
10  9   0.001    0.01     0.00      0 0 0 0 0;
4  10   0.0      0.0167   0.00      0 0 0 0 0;
11 10   0.0025   0.025    0.00      0 0 0 0 0;
3  11   0.0      0.0167   0.00      0 0 0 0 0];

mac_con = [1 1 900  0.2  0.0025  1.8  0.3  0.25  8.0  0.03  1.7  0.55
           0.25  0.4  0.05  6.5   0  0  1  0  0  1  1];
```

```
2 2 900 0.2 0.0025 1.8 0.3 0.25 8.0 0.03 1.7 0.55
0.25 0.4 0.05 6.5 0 0 2 0 0 1 1;
3 3 900 0.2 0.0025 1.8 0.3 0.25 8.0 0.03 1.7 0.55
0.25 0.4 0.05 6.175 0 0 3 0 0 1 1;
4 4 900 0.2 0.0025 1.8 0.3 0.25 8.0 0.03 1.7 0.55
0.25 0.4 0.05 6.175 0 0 4 0 0 1 1];

exc_con = [0 1 0.01 200 0 10 1 15 -15; ...
           0 2 0.01 200 0 10 1 15 -15; ...
           0 3 0.01 200 0 10 1 15 -15; ...
           0 4 0.01 200 0 10 1 15 -15];

%*****
```

The command ‘svm_mgen’ is run at the command line with the data in the correct path. The program returns the state-space matrices of the system.

REFERENCES

Ahmed S.S., Chen L. and Petroianu A. (1996). "Design of suboptimal H_∞ excitation controllers." *IEEE Transactions on Power Systems* **Vol.11**(No.1): 312-318.

Balas G.J, Doyle J.C, Glover K and Packard A and Smith R. ' μ ' Analysis and synthesis toolbox. The Mathworks Inc (1990).

Boje E, Nwokah ODI and Jennings G. (1999). "Quantitative design of SMIB power system stabilizers using decoupling theory." *1999IFAC World Congress*, Beijing, China 5-9 July 1999, **Vol O**, 267-272.

Boje E (2001a). "Non-Diagonal Controllers in MIMO Quantitative Feedback Design." *International Journal of Robust and Nonlinear Control, Isaac Horowitz Special Issue(Part 2)*, **Vol 12**, (No. 4), April 2002, 303-320

Boje E, (2001b). "Multivariable quantitative feedback design for tracking error specifications." *Automatica* **Vol. 38**: 131-138.

Boje E, (2001c). "Quantitative feedback theory for uncertain multivariable systems" '*Lecture notes-Multivariable control*'. – Private communication

Boje E and Jennings G. (2001). "Quantitative feedback design of robust power system stabilizers for single machine-infinite bus problems." *Southern African Universities Power Engineering Conference 2001* , University of Cape Town, January 2001: 103-106.

Borghesani C., Chait Y., and Yaniv O. (1994). '*Quantitative Feedback Theory Toolbox*', The Mathworks Inc. Natick, Mass.

Chonco N.S., Rigby B.S. and Harley R.G. (2000). "Damping of power system oscillations using an inverter-based controllable series compensator." Proceedings of the ninth Southern African Universities Power Engineering Conference: 192-196.

Chonco N.S. (2000). 'The application of controllable inverter-based series compensation to power oscillation damping'. Electrical Engineering, University of Natal, Durban

Cui S., Ukai H., Kando H., Nakamura K. and Fujita H. (1999). "Decentralized control of large power systems by H_{∞} control based excitation control system." IFAC 14th World congress: 255-260.

DeMello F.P. and Concordia C. (1969). "Concepts of synchronous machine stability as affected by excitation control." IEEE Transactions on Power Apparatus and Systems **Vol. PAS-88**(No.4): 316-329.

Djukanovic M., Khammash M., and Vittal V. (1998). "Application of the structured singular value theory for robust stability and control analysis in multimachine power systems." IEEE Transactions on Power Systems **Vol 13**(No. 4): 1311-1322.

García-Sanz M and Egaña I. "Quantitative non-diagonal controller design for multivariable systems with uncertainty." International Journal of Robust and Nonlinear Control, Isaac Horowitz: Special Issue(Part 2), **Vol 12**, (No. 4), April 2002, 321

Horowitz I. (1979). "Quantitative synthesis of uncertain multiple input-output feedback systems." Int. Journal of Control **Vol.30**(No.1): 81-106.

Horowitz I.M. (1993). Quantitative Feedback Design Theory, (QFT) Vol 1 . Boulder, Colorado, 80303: QFT Publications, 4470 Grimell Avenue

Kelemen M. and Akhrif O. "Linear QFT Control of a Highly Nonlinear Multi-machine Power System." International Journal of Robust and Nonlinear Control, Isaac Horowitz Special Issue(Part 2), Vol 12, (No. 4), April 2002, 961

Klein M., Rogers G.J. and Kundur P. (1991). "A fundamental study of inter-area oscillations in power systems." IEEE Transactions on Power Systems Vol 6(No. 3): 914-921.

Klein M., Rogers G.J., Moorty S. and Kundur P. (1992). "Analytical investigation of factors influencing power system stabilizers performance." IEEE Transactions on Energy Conversion Vol 7(No.3): 382-390.

Klein M., Le L.X., Rogers G.J., Farrokphay S. and Balu N.J. (1994). " H_{∞} damping controller design in large power systems." IEEE Transactions on power systems Vol 10(No.1): 158-164.

Kundur P. (1994). Power System Stability and Control. Toronto, McGraw-Hill.

Kwakernaak H. (1993). "Robust control and H_{∞} optimisation." Automatica Vol 29(No.2): 255-273.

Lakmecharan K. and Coker M.L. (1999). "Optimal placement and tuning of power system stabilizers." IEEE Transactions on Power Systems: 793-798.

Larsen E.V. and Swann D.A. (1981). "Applying power system stabilizers: parts 1-111." IEEE Transactions on Power Apparatus and Systems Vol PAS-100(No.6): 3017-3046.

Maciejowski J.M. (1989). Multivariable feedback design. U.K, Addison-Wesley Publishing Company.

Martins N.J and Lima L.T.G. (1990). "Determinations of suitable locations for power system stabilisers and Static VAR compensators for damping electro-mechanical oscillations in large power systems." IEEE Transactions on Power Systems Vol **PWRS-5** (No. 4): 1455-1469.

Rao P.S. (1998a). 'On the design of robust power system damping controllers'. Electrical Engineering. Bangalore, IIT: 264.

Rao P.S. and Sen I. (1998b). "A QFT-based robust SVC controller for improving the dynamic stability of power systems." Electric Power Systems Research Vol **46**: 213-219.

Rao P.S. and Boje E.S. (2001). "A note on the use of the structured singular value in decentralised control." 5th International Symposium on Quantitative Feedback Theory and Robust Frequency Domain Methods-Pamplona, Spain. August 2001, 107-112.

Rao.P.S. and Boje.E.S. (2002). "A quantitative design approach to PSS tuning." - Unpublished

Rigby B.S. (2000). 'Lecture notes - Power System Dynamics (2000).'

Rios M., Hadjsaid N., Feuillet R. and Torres A. (1999). "Power systems stability robustness evaluation by ' μ ' analysis." IEEE Transactions on Power Systems Vol **14**(No.2).

Rogers G. (1993). Power system toolbox, Cherry Tree Scientific Software.

Rogers G. (2000). Power system oscillations, Kluwer Academic Press.

Sedigh.A.K and Alizadeh.G (1994). "Design of robust power system stabilizers (PSS) using quantitative feedback theory." *IEE conference publication - Control,1994*(389): 416-421.

Swift F.J. and Wang H.F. (1996a). "Application of the controllable series compensator in damping power system oscillations." *IEE Proceedings-Generation, Transmission and Distribution* **Vol 143**(No. 4): 359-364.

Swift F.J., Wang H.F., and Li M. (1996b). "Analysis of controllable series compensator to suppress power system oscillations." *IEE - Sixth International conference , AC and DC power transmission* (No. 423): 202-207.

Wong D.Y., Rogers G.J. and Porreta B. (1988). "Eigenvalue analysis of very large power systems." *IEEE Transactions on Power Systems* **Vol 3**(No.2): 472-480.

Yang T.C., Zhang J.H. and Yu H. (1999). "A new decentralized controller design method with application to power system stabilizer design." *Control engineering practice* **Vol 7**: 537-545.

Yaniv O. (1999). *Quantitative feedback design of linear and nonlinear control systems*, Kluwer Academic Publishers.
